Economic Geology

BULLETIN OF THE SOCIETY OF ECONOMIC GEOLOGISTS

VOL. 103 March–April 2008 NO. 2

Fluid Inclusion Evidence for Magmatic-Hydrothermal Fluid Evolution in the Porphyry Copper-Molybdenum Deposit at Butte, Montana

BRIAN G. RUSK[†,*] MARK H. REED,

Department of Geological Sciences, 1272 University of Oregon, Eugene, Oregon, 97403

AND JOHN H. DILLES

Department of Geosciences, 104 Wilkinson, Oregon State University, Corvallis, Oregon, 97331

Abstract

The porphyry Cu-Mo deposit in Butte, Montana, formed where magmatic hydrothermal fluids, introduced with injections of porphyrytic dikes, fractured and permeated the Butte Quartz Monzonite. These fluids formed a stockwork of quartz and quartz-sulfide veinlets with a variety of styles of potassic and sericitic alteration envelopes. The distribution of vein and alteration types and the distribution of fluid inclusions in these veins record the progressive pressure, temperature, and compositional evolution of the hydrothermal fluids that formed this world-class deposit.

Deep drilling and 1,300 m of offset along the Continental fault provide a vertical view of almost 3 km through the Butte deposit. Deep veins within and below the highest Mo grades are quartz dominated with thin K-feldspar or, less commonly, biotitic alteration rims. Fluid inclusions in deep veins trapped a single phase aqueous fluid containing 2 to 5 wt percent NaCl equiv and 2 to 8 mol percent CO_2 at temperatures between 575° and 650°C and pressures between 200 and 250 MPa, corresponding to depths between 6 and 9 km. Although Cu grades are low in this region, abundant chalcopyrite daughter minerals in fluid inclusions indicate that the fluids were Cu rich. Fluids that formed these veins transported Cu from the magma below, upward into the region of Cu mineralization with only minor Cu precipitation.

Over a kilometer above the bulk of deep quartz and quartz-molybdenite veins, the highest Cu grades are in and around chalcopyrite-bearing quartz-sulfide veins with biotitic alteration (early dark micaceous veins), and their upward, equivalent magnetite-chalcopyrite-pyrite-quartz veins with wide K-feldspar, green sericite, and chlorite alteration (pale-green sericitic veins). These veins contain more evidence for brine-vapor unmixing than any other vein type. The upward progression of early dark micaceous veins to pale-green sericitic veins formed where low salinity, CO_2-bearing fluids, similar to those trapped in deep quartz veins, ascended, depressurized, sometimes unmixed, and cooled from ~650°C at 90 MPa to ~475°C at ~50 MPa.

As low salinity, CO_2-bearing, aqueous fluids, similar in composition to fluids trapped in deep quartz veins, cooled at shallow depths, they formed late pyrite-quartz veins with sericitic alteration. These veins formed from fluid cooling at temperatures between 370° and 450°C at transiently hydrostatic pressures between 40 and 70 MPa, corresponding to depths of 4 to 7 km. Most pyrite-quartz veins formed at pressures and temperatures above the H_2O-NaCl-CO_2 solvus, but evidence for brine-vapor unmixing is also present. Pyrite-quartz veins formed at progressively greater depths as the hydrothermal system cooled, overprinting much previous mineralization.

Late Cu-Pb-Zn-Ag-As-rich Main stage veins formed from dilute fluids containing <3 wt percent NaCl equiv and <2 mol percent CO_2. These fluids were trapped between 230° and 400°C under hydrostatic pressures between 20 and 60 MPa and depths of 2 to 6 km. No evidence of boiling is observed in Main stage veins.

Fluid inclusion phase relationships indicate that the Butte porphyry Cu-Mo deposit formed at 5 to 9 km depth, greater than any other porphyry-type deposit. At Butte, the similarity in bulk composition of fluids trapped in early quartz-rich veins with potassic alteration and late pyrite-quartz veins with sericitic alteration implies that an underlying magma continually provided low salinity, CO_2-bearing fluids of relatively constant composition during the entire life of the hydrothermal system. We hypothesize that rather than resulting from changes in fluid chemistry due to magma crystallization, the entire suite of vein and alteration types and the ore metal distribution reflect the path of cooling, depressurization, and wall-rock interaction of a parental magmatic-derived fluid of relatively constant initial composition.

[†] Corresponding author: e-mail, bgrusk@usgs.gov

[*] Present address: School of Earth and Environmental Sciences, James Cook University, Townsville, Queensland, 4810, Australia.

©2008 by Economic Geology, Vol. 103, pp. 307–334

0361-0128/08/3727/307-28

Fluid inclusions, vein and alteration relations, and ore metal distribution indicate that Cu and Mo were introduced into the hydrothermal system by the same fluids, but that the mechanisms of precipitation of these metals were decoupled. Early dark micaceous and, to a greater extent, pale-green sericitic, veins have wide alteration envelopes and contain more evidence for fluid unmixing than any other vein type, which suggests that chalcopyrite precipitation was driven by a combination of fluid unmixing, fluid-rock reaction, and fluid cooling between 650° and 475°C. Most molybdenite mineralization, however, is in quartz-dominated veins with little or no alteration that are dominated by low salinity inclusions. These veins formed in response to pressure decrease rather than cooling. After chalcopyrite and molybdenite precipitation, low salinity fluids cooled, usually at temperatures and pressures above the H_2O-NaCl-CO_2 solvus, to produce significant acid and voluminous sericitic alteration accompanied by pyrite-quartz vein formation that overprints much of the deposit and contains anomalous but noneconomic Cu.

Introduction

Porphyry Cu (Mo-Au) deposits form in the upper crust, where fluid overpressures generated in the cupola of a crystallizing magma hydrofracture the overlying rock (Burnham, 1979), allowing magma and fluids to intrude, forming porphyry dikes surrounded by stockwork fractures. Aqueous fluids permeate the fractured rock where the fluids depressurize, cool, and chemically react with wall rock, forming veins with alteration envelopes. Magmatic volatiles enriched in incompatible elements precipitate sulfides of Cu and Mo in addition to quartz.

Porphyry Cu deposits from around the world and of all ages show similar vein and alteration types and similar patterns of vein and alteration distribution (Gustafson and Hunt, 1975; Beane and Bodnar, 1995; Seedorff et al., 2005). Alteration is typically zoned from an inner K-silicate assemblage outward to propylitic alteration, with later sericitic alteration cutting the K-silicate zone or lying near the potassic-propylitic interface (Lowell and Guilbert, 1970; Gustafson and Hunt, 1975; Beane and Titley, 1981; Seedorff et al., 2005). Commonly, early Cu-bearing quartz veins with K-silicate alteration are cut by quartz-molybdenite veins, which are cut by pyrite veins with sericitic alteration (cf. Gustafson and Hunt, 1975). In some deposits, late veins with advanced argillic and sericitic alteration cut all of the above vein types (Meyer et al., 1968; Lowell and Guilbert, 1970; Corn, 1975; Arribas et al., 1995; Phillips et al., 1998; Ossandon et al., 2001; Manske and Paul, 2002; Khashgerel et al., 2006).

Fluid inclusions in vein quartz from porphyry Cu deposits trap fluids with a wide range of compositions under a wide range of pressure and temperature conditions. In a single deposit, hydrothermal fluids may originate from magmatic, sedimentary, or meteoric water sources (Bowman et al., 1987; Dilles, 1987), and fluid salinities may range from 0 to 70 wt percent NaCl equiv. CO_2 has been identified in inclusions from some deposits, but other gases such as H_2S, N_2, and CH_4 are typically not detected. Temperatures of vein formation range from ~300° to ~800°C, and pressures vary from hydrostatic to lithostatic, typically ranging from <10 to ~150 MPa, corresponding to depths between 1 and 5 km and fluid densities from <0.1 to >1.3 g/cm^3.

Owing to superposition of multiple mineralizing events, fluid inclusions that trapped fluids of different compositions at different times are commonly juxtaposed within a single vein. Such superposition complicates the interpretation of fluid origin and evolution by obscuring temporal relationships between fluid inclusions, vein minerals, and alteration minerals (cf. Rusk and Reed, 2002; Redmond et al., 2004; Seedorff and Einaudi, 2004; Seedorff et al., 2005). Therefore, some ambiguity remains as to the relationship between low salinity and high salinity fluid inclusions and the origin and evolution of these fluids. For example, previous fluid inclusion studies in many porphyry Cu deposits suggest that early K-silicate alteration that accompanies Cu and Mo mineralization is produced by high salinity, high-temperature magmatic fluids. However, low to moderate salinity fluids are implicated in K-silicate alteration in some deposits (Redmond et al., 2004; this study). Later sericitic alteration has been interpreted to have been produced by low salinity, low-temperature meteoric fluids (Sheppard and Taylor, 1974; Beane and Titley, 1981; Beane and Bodnar, 1995; Taylor, 1997); however, a magmatic fluid origin of pyrite veins with sericitic alteration has been inferred more recently in many deposits (Hedenquist et al., 1998; Zhang et al., 1999; Watanabe and Hedenquist, 2001; Ulrich et al., 2001, Seedorff and Enaudi, 2004; this study) and high salinity, magmatic fluid inclusions have been identified in sericitic alteration at Henderson, Colorado (Seedorff and Einaudi, 2004); Endeavor 26 North, Australia (Harris and Golding, 2002); Gaby Sur, Chile (J. Dilles, unpub. data); and Butte, Montana (this study).

Halite-saturated inclusions are ubiquitous in porphyry Cu deposits and low-density vapors are also extremely common. However, in most deposits, it is unclear whether these fluids directly exsolved from a magma or whether they were generated by fluid unmixing. Where brine and vapor are generated by fluid unmixing, the composition of the parental hydrothermal fluids is typically unknown. In the vast majority of porphyry Cu deposits, it is therefore difficult to determine how the compositions of hydrothermal fluids change with time and how those changes affect ore mineral distribution and alteration zonation. Models of the physical and chemical processes that form porphyry Cu deposits based on fluid inclusions are compromised in the absence of identification of the parental magmatic hydrothermal fluids from which unmixed fluid inclusion populations are derived.

In previous fluid inclusion investigations at Butte, Roedder (1971) showed that some veins contain halite-bearing inclusions, but Roberts (1975) identified abundant low salinity fluid inclusions in deep, early veins trapped at high temperature and pressure. The presence of chalcopyrite daughter minerals in these inclusions led him to infer that low salinity, Cu-rich fluids were responsible for most Cu mineralization. Our investigation was designed to determine whether these low salinity fluids were the parental magmatic-hydrothermal fluids and to examine how fluid properties evolved spatially and temporally during the life of the hydrothermal system. We have reconstructed the physical and chemical evolution of

the hydrothermal system that formed the porphyry Cu-Mo deposit in Butte on the basis of vein and alteration mineral content, vein cutting relations, and fluid inclusion distribution and analysis. These data are discussed in the context of the evolution of the pressure, temperature, and fluid compositions of the magmatic-hydrothermal system in space and time. Our results provide constraints on the role of fluctuations in fluid pressure, temperature, and composition on vein formation, wall-rock alteration, and metal precipitation.

Methods

Field mapping

Over 5,000 m of drill core was logged at a scale of 1:240, and about 1,000 core samples containing various vein and alteration types from various depths were collected for laboratory analyses. Most samples are from 10 deep drill holes that penetrate the Pittsmont dome and the adjacent zone of pervasive gray sericitic alteration to depths between 1,200 and 2,600 m below the surface. We also collected and analyzed some samples from the Anaconda dome, including both core and hand samples taken by mine geologists over the past 100 years. A few samples were collected during several short excursions into the Continental Pit, but detailed mapping of bench faces in the active Continental Pit was not possible.

Fluid inclusion sampling

Over 200 samples were observed for inclusion type, abundance, spatial distribution, and size. Approximately 50 of these samples were further analyzed by microthermometry, SEM-EDS daughter-mineral analysis, and/or Raman spectroscopy. Many of these samples were previously examined using scanning electron microscope cathodoluminescence (Rusk and Reed, 2002; Rusk et al., 2006), fluid inclusion trace element analysis by laser ablation-inductively coupled plasma-mass spectrometry (LA-ICP-MS) (Rusk et al., 2004), and analyses of fluid inclusion solutes, gases, and noble gas isotopes (Rusk et al., 2005). Over 3,000 inclusions were analyzed by microthermometry. The inclusions range from less than 1 to ~80 μm in diameter, with the vast majority of inclusions being less than 5 μm. Most inclusions analyzed by microthermometry were between 5 and 20 μm in diameter.

Microthermometry

Microthermometry was carried out on Fluid Inc-adapted U.S. Geological Society Gas-Flow Heating/Freezing Systems at the University of Oregon and Oregon State University. Thermocouples were calibrated at –56.6°, 0.0°, and +374.1°C using synthetic fluid inclusions. The precision of temperature measurements on cooling runs is about ±0.1°C. On heating runs, the precision is ±2°C. Ice-melting temperatures were observed at a heating rate of no more than 0.1°C/s. Homogenization temperatures were observed at a heating rate of ≤1°C/s. Homogenization of halite-bearing inclusions was obtained on only one assemblage of halite-bearing inclusions per sample chip to avoid analyzing inclusions that stretched due to previous heating. Heating cycles of about 5°C were used to determine the homogenization temperature of bubble and halite in halite-bearing inclusions. Heating cycles also constrained the melting temperature of clathrate to within ±0.2°C in most CO_2-bearing inclusions.

Scanning electron microscope-energy dispersive spectrometry

Daughter minerals in fluid inclusions were identified by scanning electron microscope-energy dispersive spectrometry (SEM-EDS) of opened fluid inclusions. SEM-EDS analyses and secondary electron (SEM-SE) images were acquired on carbon-coated broken quartz fragments at beam currents between 0.05 and 5 nAmps, and electron acceleration potentials of 5 to 20 kV. Opened fluid inclusions were identified on broken quartz fragments (shattered with a hammer and chisel in liquid nitrogen to avoid ejection of daughter minerals) with secondary electron imaging, and elemental compositions of daughter minerals were determined by SEM-EDS.

Raman spectroscopy

Carbon dioxide contents of fluid inclusions were estimated using Raman analysis and the technique of Azbej et al. (2007) at Virginia Polytechnic Institute. With this technique, inclusions are homogenized in a Chaixmeca heating stage mounted on a microscope attached to a Dilor XY Raman microprobe. Excitation is provided by an Ar-ion laser, with a laser power of approximately 10 mW measured at the sample. The ratio of the area under the CO_2 peak at 1,388 cm^{-1} to the area under the H_2O peak at about 3,500 cm^{-1} varies linearly with CO_2 content over the range from about 0 to 25 mol percent CO_2. The precision and accuracy of the Raman technique for determining the CO_2 content of homogenized inclusions is estimated to be better than ±1 mol percent over the range of concentrations of inclusions in this study.

Fluid inclusion references

Salinities, CO_2 contents, and densities in liquid-vapor inclusions that formed clathrate upon cooling were estimated using the computer program ICE (Bakker, 1997) and the data of Duan et al. (1992a, b). Salinities in CO_2-bearing inclusions that did not form clathrate upon cooling were estimated using the technique of Hedenquist and Henley (1985). Salinities of inclusions containing halite, liquid, and vapor at room temperature were estimated using the data and methodology of Bodnar and Vityk (1994). For inclusions that homogenize by halite dissolution, this method underestimates salinity by up to 3 wt percent NaCl equiv (Bodnar and Vityk, 1994). Salinities in liquid plus vapor inclusions that are inferred to contain no CO_2 were estimated using the data of Bodnar (1993). Isochores were calculated for CO_2-bearing inclusions using the program MACFLINCOR (Brown, 1989) and the data of Bowers and Helgeson (1983), which are in close agreement with lines of constant homogenization temperature predicted by the equation of state of Duan et al. (1995). For inclusions that contain neither CO_2 nor halite, isochores were calculated with the program MACFLINCOR using the data of Bodnar and Vytik (1994).

Geologic Background

The deposit at Butte provides an exceptional opportunity to understand the physical and chemical evolution of a hydrothermal system that formed a porphyry Cu deposit. The deposit geology has been studied for more than 100 years (Brown, 1894; Emmons and Tower, 1897; Weed, 1912; Sales, 1914; Sales and Meyer, 1948; Meyer, 1965; Meyer et al., 1968; Miller, 1973; Roberts, 1975; Brimhall, 1977). The host rock is

uniform throughout the deposit and provides a uniform backdrop for alteration and zoning such that variations in physiochemical processes due to rock composition are absent. Ten deep drill holes, including one in the upthrown block east of the Continental fault, reach depths equivalent to ~2,600 m below the present surface. The unusually great depth at which the deposit formed (Roberts, 1975; this study) and the large horizontal and vertical distance over which samples were collected allow exceptional insights into the physical and chemical processes of this magmatic-hydrothermal system.

The porphyry Cu and base metal lode deposits at Butte are hosted by the Butte Quartz Monzonite at the southern end of the Boulder batholith (Meyer et al., 1968; Smedes, 1973; Tilling, 1973) (Fig. 1). The ~76 m.y. old Butte Quartz Monzonite (Tilling et al., 1968; Martin et al., 1999; Lund et al. 2002) intrudes Proterozoic sedimentary rocks of the Belt Supergroup and to the south of Butte, Archean crystalline basement. The Butte Quartz Monzonite is medium to coarse grained and is uniform in mineral content throughout the Butte district. Quartz and K-feldspar, in roughly equal amounts, comprise 40 to 45 vol percent of the Butte Quartz Monzonite. Plagioclase constitutes 35 to 40 vol percent, and biotite and hornblende with accessory magnetite, titanite, ilmenite, and apatite make up the remaining 15 to 20 vol percent of the pluton (Meyer et al., 1968; Roberts, 1975). The oxide and titanite-bearing assemblages suggest an elevated magmatic oxygen fugacity (~NNO + 2: Field et al., 2005). Sheeted granoaplite dikes and local pegmatite dikes form subhorizontal sheets within the Butte Quartz Monzonite (Houston, 2002).

The Butte Quartz Monzonite, aplites, and pegmatites are cut by a swarm of east-west–striking, steeply south dipping quartz porphyry dikes that contain phenocrysts of plagioclase, biotite, K-feldspar, and partially resorbed quartz. U/Pb zircon ages of several dikes yield ages of ~66 ± 1 Ma (Lund et al., 2002). Chalcopyrite- and pyrite-bearing biotitic breccias emanating from these dikes grade into biotitic veins, indicating that hydrothermal fluids were introduced with dike intrusion about 10 m.y. after emplacement of the Butte Quartz Monzonite. Several biotitic breccias from the Continental and Berkeley Pits (Fig. 1) contain fragments of quartz veins, indicating that some deep veins formed before the intrusion of some dikes. The number of intrusive events at Butte and their relation to mineralization ore is not well constrained, nor is the duration of dike intrusion. The source stock or cupola from which these dikes originated has not been identified, although the two deepest drill holes intersect a texturally distinct rock that may be the uppermost portion of a cupola.

Two distinct stages of mineralization are identified at Butte. "Pre-Main stage" porphyry Cu-Mo stockwork veins are cut by "Main stage" veins, which are large, through-going Cordilleran-style base metal lodes containing Cu-, Zn-, Pb-, and Ag-sulfides (Meyer et al., 1968) (Fig. 2). The spatial overlap of the pre-Main stage and Main stage mineralization suggests that the two events are related; however, Main stage veins always cut pre-Main stage veins, and the genetic relationship between the two stages remains the subject of some debate. This study concentrates on pre-Main stage veins; however, a few Main stage veins were analyzed for completeness.

Mine exposures and deep drilling reveal that pre-Main stage mineralization at Butte consists of two internally zoned domes of Cu and Mo mineralization that are both about 2 km in diameter (Reed, 1999; Reed and Rusk, 2001) (Fig. 3). The

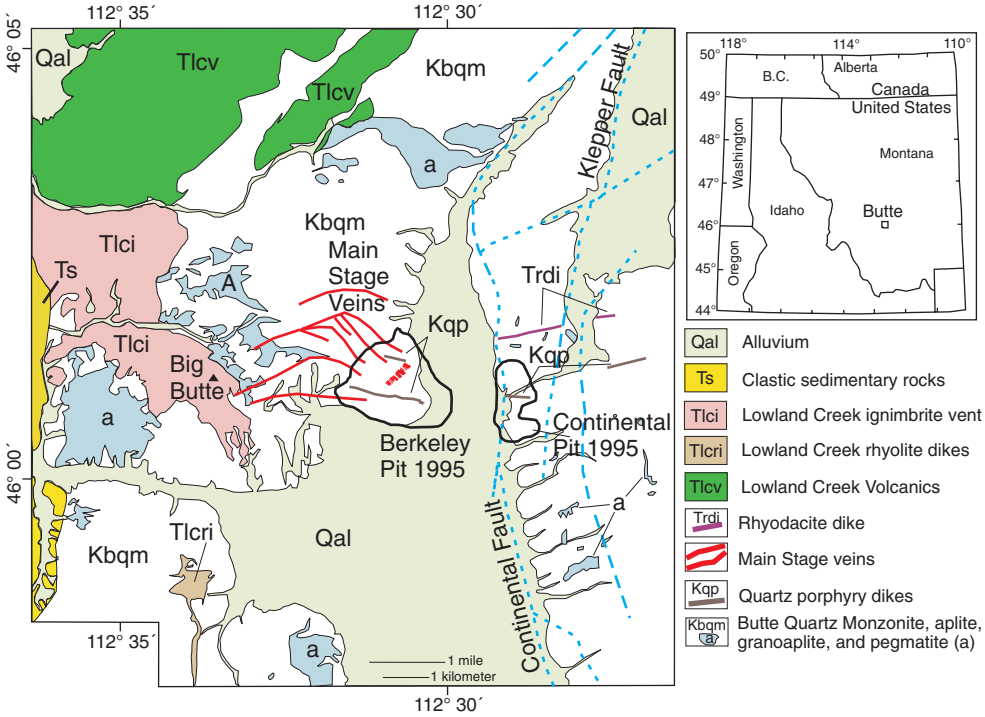

FIG. 1. Location map and regional geologic setting of the Butte district, modified from Houston (2002), Proffett (1973), and unpublished reports of the Anaconda Company. The porphyry Cu deposit lies entirely within the Butte Quartz Monzonite and related aplites, granoaplites, and pegmatites.

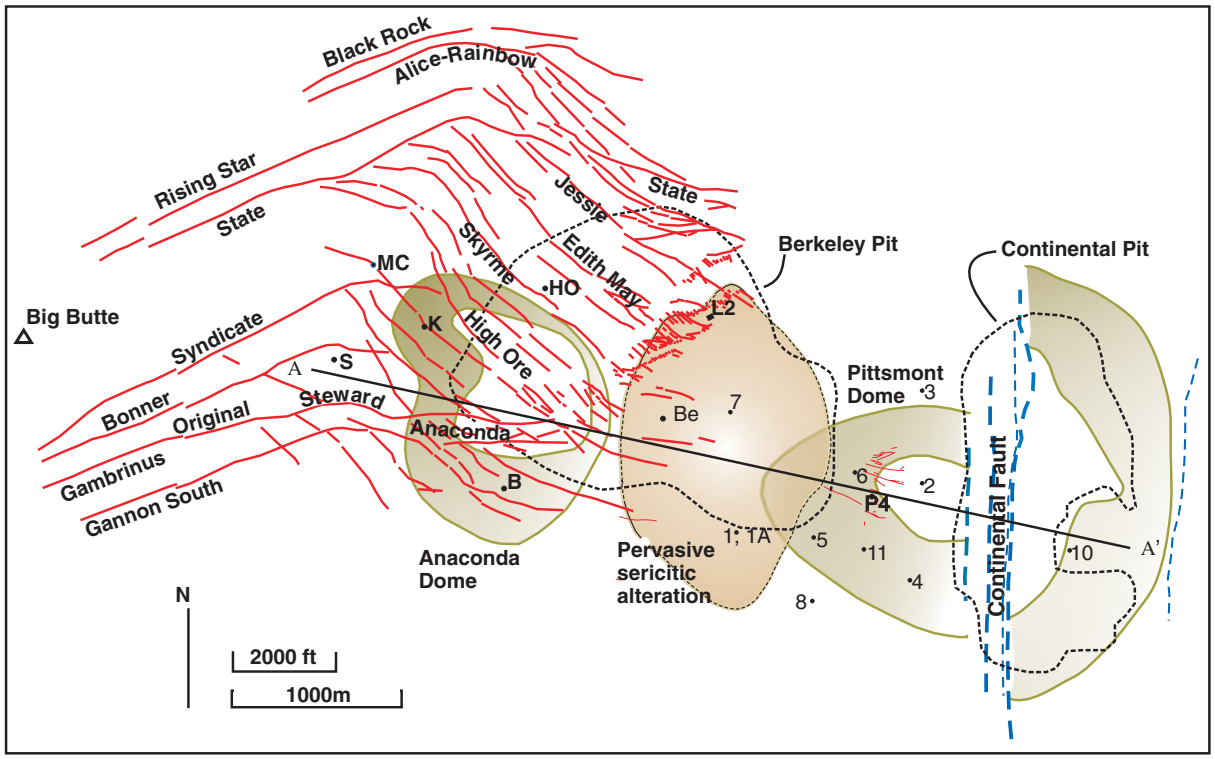

FIG. 2. Map of the Main stage and pre-Main stage mineralization at Butte. The subsurface trace of the Main stage veins is shown in red, and the subsurface position of pre-Main stage porphyry Cu centers the Pittsmont and Anaconda domes are shown in green. Also in the subsurface, a zone of pervasive sericitic alteration separating the two porphyry Cu mineral centers is shown in tan. The locations of 10 deep drill holes sampled for this study are numbered in the Pittsmont dome. The locations of several mine shafts are also indicated: S = Steward, K = Kelly, MC = Mountain Consolidated, Be = Berkley, HO = High Ore, L2 = Leonard, P4 = Pittsmont #4, and B = Belmont. Cross section A-A' is shown in Fig. 3.

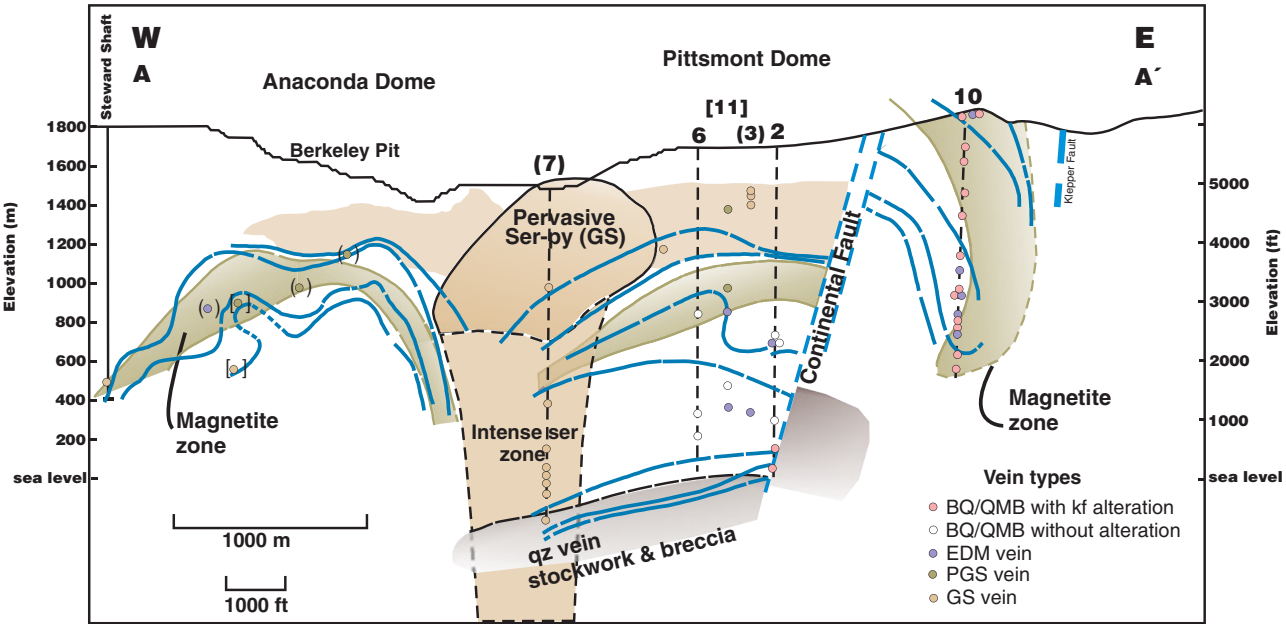

FIG. 3. East-west geologic cross section (A-A' in Fig. 2) of pre-Main stage porphyry Cu-Mo mineralization at Butte. The two mineral centers are the Anaconda dome in the west, and the Pittsmont dome in the east. These domes are defined by a zone of abundant magnetite veins and by Mo grade contours (shown in blue). Separating these two domes is a bulb-shaped body of rock that is pervasively altered to quartz, sericite, and pyrite. The Continental fault displaces the eastern part of the Pittsmont dome upward by ~1,300 m. Colored circles represent locations of many of the samples used in microthermometric studies. See Table 1 for abbreviations. [ ] indicate samples or drill holes located in front of the section; () indicate samples and drill holes located behind the section.

two domes, the Anaconda in the west and the Pittsmont in the east, are defined by a zone of abundant magnetite-bearing veins and by Mo grade contours. Separating these two domes is a bulb-shaped zone, up to 1.2 km wide, of intense pyritic veining and pervasive gray sericitic alteration. The zone of pervasive gray sericitic alteration extends below the level of deepest drilling at a depth of more than 2 km below the bottom of the Berkeley Pit.

Both domes are concentrically zoned with widely overlapping shells of alteration bordering centimeter-scale stockwork veins. The same vein and alteration types and vein-cutting relationships are observed in both domes. The innermost concentric zone of mineralization, which is observed only in the deepest drilling of the Pittsmont dome, consists of a stockwork of barren quartz veins with minor molybdenite and thin K-feldspar alteration haloes. Also abundant in this zone are numerous centimeter-scale, discontinuous, irregular aggregates and pods of quartz in intensely sericitized Butte Quartz Monzonite and quartz porphyry (Fig. 4K). This core of barren quartz veins may be present in the Anaconda dome as well, but mine workings and drill holes do not penetrate deeply enough to reveal it. Upward and outward from the barren quartz vein stockwork, but below the bulk of chalcopyrite and magnetite mineralization, molybdenite grades are highest. This region is characterized by quartz-dominated veins containing a few percent molybdenite and no alteration. These veins cut early dark micaceous veins (Meyer, 1965; Brimhall, 1977), which consist of quartz-chalcopyrite-pyrite veins with biotite-K-feldspar-sericite-quartz alteration veins from the next outward zone. Early dark micaceous alteration yields upward to a 300-m-thick shell of abundant quartz-chalcopyrite-magnetite-pyrite veins with K-feldspar, chlorite, quartz, and pale-green sericitic alteration envelopes (Reed, 1999; Reed et al., 2005). Both early dark micaceous and pale-green sericitic veins are cut by barren quartz and quartz-molybdenite veins in the two domes. Above the zone of abundant quartz-chalcopyrite-magnetite-pyrite veins is the sparse gray sericite zone where pyrite-quartz veins have alteration envelopes dominated by quartz, sericite, and pyrite (Reed, 1999; Geiger et al., 2002; Rusk and Reed, 2002). Pyrite-quartz veins with sericitic alteration cut all other pre-Main stage vein types in both domes and in the central pervasively sericitized bulb (Fig. 3). In the outermost zone, veins contain pyrite, sphalerite, galena, rhodochrosite, chalcopyrite, and epidote in K-feldspar–bearing propylitic alteration. The age relationships and distribution of propylitic veins and alteration are poorly studied. Most Main stage veins are above and west of the Anaconda dome (Fig. 2).

In the eastern part of the deposit, the north-striking, 55° west-dipping, postore Continental fault normally offsets the Pittsmont dome by approximately 1,250 m (Meyer et al., 1968; Ratcliff, 1973; Reed, 1999). One deep drill hole was collared in the upthrown Continental block east of the fault (DDH 10, Fig. 3). Including the 1,250 m of throw on the fault, the bottom of this hole reaches an equivalent depth of ~2,600 m below the surface west of the Continental fault. Rocks from the drill hole east of the Continental fault were only locally affected by later, cooler fluids that overprinted much of the deposit west of the Continental fault. Few pyrite-quartz or Main stage veins exist in the lower 1,000 m of this drill hole.

Veins and Wall-Rock Alteration

Early dark micaceous veins

Early dark micaceous veins (Fig. 4F, G; Table 1) are quartz-sulfide veins with alteration envelopes containing biotite, K-feldspar, quartz, and sericite (Meyer, 1965; Roberts, 1975; Brimhall, 1977). Pyrite, chalcopyrite, and magnetite are present in these veins, but are more common in the alteration envelopes. At moderate and shallow depths, early dark micaceous veins are the earliest vein type recognized. Here, the distinction between early dark micaceous veins and barren quartz and quartz-molybdenite veins is clear; early dark micaceous veins contain chalcopyrite and have wide alteration envelopes, whereas barren quartz and quartz molybdenite veins have little or no chalcopyrite or alteration envelopes. However, deep in the quartz-rich core of the deposit, the distinction between the two vein types is vague. Here, early dark micaceous veins are quartz dominated, chalcopyrite poor, and some contain anhydrite, K-feldspar, and/or molybdenite. Like barren quartz and quartz-molybdenite veins from this depth, alteration envelopes around these veins are less than a few millimeters in width and, in addition to the minerals mentioned above, some contain anhydrite, corundum, andalusite, and plagioclase of two compositions (An_{22}-An_{30} and An_{1}-An_{7}, possibly reflecting the peristerite gap). Some deep, early dark micaceous veins cut some deep barren quartz and quartz-molybdenite veins, a relationship not observed at shallower depths.

In moderate and shallow early dark micaceous alteration envelopes, alteration envelopes are typically a few centimeters in width, sericite is more abundant, and anhydrite, corundum, and plagioclase are not observed. Shallower early dark micaceous veins typically contain more pyrite, chalcopyrite, and magnetite, both in the vein and in the alteration envelope, than do deep, early dark micaceous veins.

Pale-green sericitic veins

Upward and outward from early dark micaceous-type veins, but also overlapping with them, are veins containing magnetite, chalcopyrite, pyrite, and quartz, bordered by alteration envelopes dominated by K-feldspar, quartz, green sericite, chlorite, and minor calcite (Fig. 4H). Such veins are referred to as "pale green sericitic" veins (Reed, 1999; Reed and Rusk, 2001). Pale-green sericitic veins typically contain more than 50 vol percent opaques; more than do early dark micaceous or quartz-molybdenite veins. Pale-green sericitic veins also have wider alteration envelopes than other vein types, commonly extending more than 5 cm on each side of the vein. Pale-green sericitic veins are the upward extension of early dark micaceous veins and the transition from early dark micaceous- to pale-green sericitic-type alteration envelopes has been observed in underground mapping. Pale-green sericitic veins are abundant at moderate to shallow depths, and they are rare in the deep quartz-rich core of the deposit. Early dark micaceous and pale-green sericitic veins coincide with the zone of highest pre-Main stage Cu grade.

Barren quartz and quartz-molybdenite veins

The majority of barren quartz veins are deeper than the majority of quartz-molybdenite veins, and the majority of

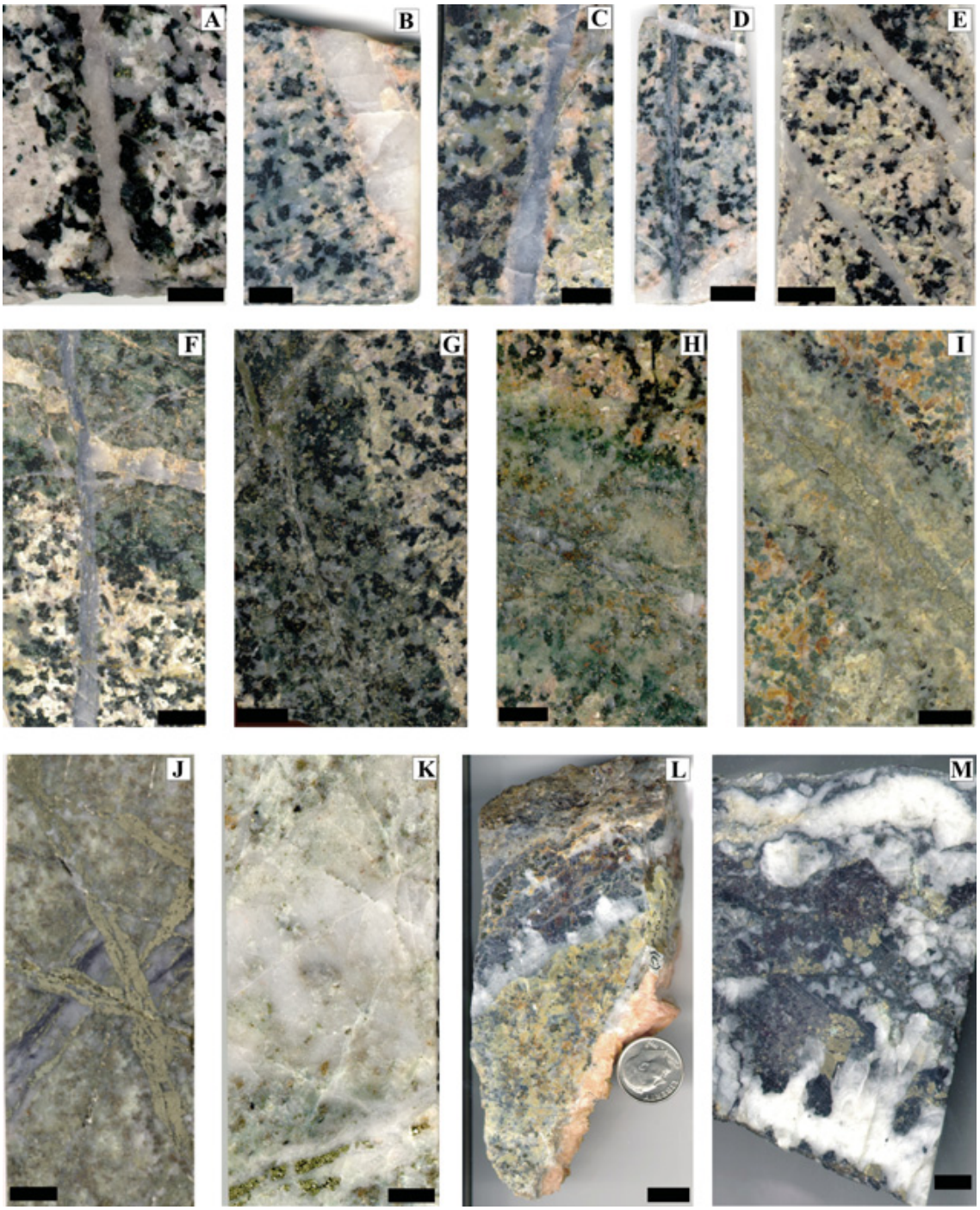

FIG. 4. Vein and alteration types from Butte (west of Continental fault, unless noted). A) Deep quartz vein with early dark micaceous (EDM) alteration from east of the Continental fault. B) Deep, barren quartz vein with pink anhydrite and K-feldspar alteration from east of the Continental fault. C) Deep quartz-molybdenite vein with K-feldspar alteration from east of the Continental fault. D) Deep quartz-molybdenite vein with minor early dark micaceous alteration (vertical vein) cut by a barren quartz vein with minor K-feldspar alteration (top of sample), but cutting another barren quartz vein with K-feldspar alteration (bottom of sample). E) Deep, barren quartz veins with minor K-feldspar alteration. F) Quartz-molybdenite vein with no alteration from moderate depth cutting a quartz-rich early dark micaceous vein. G) Quartz-chalcopyrite vein with early dark micaceous alteration from intermediate depth. H) Magnetite-chalcopyrite-pyrite vein with pale-green sericitic (PGS) alteration from intermediate to shallow depths. I) Pyrite-quartz vein with gray sericitic (GS) alteration from shallow depth. J) Pyrite veins cutting a quartz-molybdenite vein in the zone of pervasive gray sericitic alteration. Gray sericitic alteration is destructive of original Butte Quartz Monzonite texture. K) Deep pyrite-quartz vein from the quartz stockwork deep in the zone of pervasive sericitic alteration. The original rock texture has been destroyed and hydrothermal quartz is abundant but not in well-defined veins. L) Peripheral Main stage vein containing galena, sphalerite, and rhodochrosite. M) Central zone Main stage vein containing covellite, pyrite, and enargite. All scale bars are 1 cm in length.

TABLE 1. Paragenetic Sequence of Vein Types and Alteration Minerals Based on Petrography and Crosscutting Relationships

Vein type	Vein minerals[1]	Added alteration minerals	Relict igneous minerals[2]	Timing	Location
Early dark micaceous (EDM)	qz, kf, cp, ± (anh, mb, py, mt, ca, rut)	bi, ser, kf mt, cp, py, ± (plag, and, cor, ca, anh)	plag, kf, mt	Cut by BQ/QMB, GS, and MS at most depths. Cuts BQ/QMB at great depth. Contemporaneous with dike intrusion	Most abundant at intermediate depths above BQ/QMB and below PGS A few deep EDM veins exist
Pale green sericitic (PGS)	mt, cp, py, qz, ca, ± (mb, kf, rut)	plag, ser, chl, py, ca, cp, kf	kf	Cut by BQ/QMB, GS, and MS	Upward and outward from EDM veins Not common at depth Below most GS veins
Barren quartz/ Quartz-molybdenite BQ/QMB	qz,±(anh, mb, kf, ca, rut)	kf, ca, anh, bi, or none	qz, kf, plag, mt, bi	Most cut EDM and PGS veins Cut by a few deep EDM veins Cut by GS and MS veins	Dominant vein type at great depth Less common at intermediate depths Not common at shallow depths
Gray sericitic (GS)	py, qz, ±(rut)	ser, py, chl, qz		GS veins cut all above vein types	Mostly shallow; upward and outward from PGS. Present at all depths in the pervasively altered GS zone
Main stage (MS)	cv, en, bn, sl, gn, rc, py, cp, qz, and many others	ser, qz, kaol, py complex, see Meyer et al., 1968		Always cut all other vein types	Mostly shallow

[1] Mineral abbreviations are as follows: andalusite = and, anhydrite = anh, apatite = ap, biotite = bi, bornite = bn, calcite = ca, chalcopyrite = cp, chlorite = chl, covellite = cv, enargite = en, galena = gn, hornblende = hbl, K-feldspar = kf, kaolinite = kaol, magnetite = mt, molybdenite = mb, plagioclase = plag, pyrite = py, quartz = qz, rhodochrosite = rc, rutile = rut, sericite = ser, sphalerite = sl, zircon = zr

[2] Relict zr, ap, and qz in all alteration types

quartz-molybdenite veins are deeper than the majority of early dark micaceous veins. There is a continuous gradation in molybdenite concentrations from veins termed "barren quartz veins" to those termed "quartz-molybdenite veins." Nearly all barren quartz veins contain minor amounts of molybdenite, and a barren quartz vein is defined as a quartz-dominated vein where molybdenite is not observable in hand sample without a hand lens or microscope. In other respects, the two vein types are identical, and in some samples a barren quartz vein may become a quartz-molybdenite vein within a few centimeters along the vein. We therefore refer to them here as a single vein type, barren quartz–quartz-molybdenite. Barren quartz and quartz-molybdenite veins cut each other at all depths, and at moderate depths they cut pale-green sericitic and early dark micaceous veins. In deep samples from the quartz-rich core of the deposit, a few early dark micaceous veins cut barren quartz–quartz-molybdenite veins. At all depths, the latter type veins contain more than 95 vol percent quartz and less than 3 percent molybdenite. In addition, veins of this type commonly contain purple anhydrite, K-feldspar, rutile hairs, and calcite, whereas these veins at moderate depths contain only quartz, rutile hairs, and molybdenite. Deep barren quartz–quartz-molybdenite and early dark micaceous veins have a thin, K-feldspar lining separating vein quartz from wall-rock minerals (Fig. 4A-C). The K-feldspar alteration is not apparent in shallower samples (Fig. 4E, F).

Molybdenite in quartz-molybdenite veins commonly occurs in multiple bands within and parallel to bands of quartz, typically near the vein margins. In veins with the least amount of hydrothermal overprint, molybdenite grains touch anhydrite, calcite, K-feldspar, or biotite. Pyrite and chalcopyrite, where present, are commonly along discreet late fractures distinguished by cathodoluminescence. Several quartz-molybdenite veins have been identified with euhedral quartz projecting into aplitic quartz and K-feldspar intergrowths in the vein centers. Such vein dikes have been recognized in several porphyry-type deposits (White et al., 1981; Carten et al., 1988; Seedorff and Einaudi, 2004).

Gray sericitic veins

Pyrite-quartz veins (Fig. 4I, J) with gray sericitic alteration (gray sericitic veins) typically cut all of the above vein types. Most pyrite-quartz veins contain more than 80 vol percent sulfide; the highest percentage of all the pre-Main stage veins. Alteration envelopes contain muscovite, quartz, pyrite, and, in some samples, colorless (magnesian) chlorite. Cathodoluminescent images show that much of the quartz in these veins is fractured and partially dissolved Butte Quartz Monzonite quartz and earlier vein quartz overgrown by euhedral quartz projecting into pyrite (Rusk and Reed, 2002). Gray sericitic veins are common above the magnetite zone where early dark micaceous and barren quartz–quartz-molybdenite veins are rare. Gray sericitic veins also dominate the central "bulb" of pervasive quartz-sericite-pyrite alteration between the Pittsmont and Anaconda domes. In this region, gray sericitic envelopes on closely spaced pyrite veins coalesce so that the entire volume (1 km^3) of Butte Quartz Monzonite is altered to quartz, sericite, and pyrite (Fig. 3).

Main stage veins

Main stage veins are several centimeters to several meters wide and cut all other vein types. Some are laterally continuous for over 7 km across the district and were mined to depths

of greater than 1.5 km (see Meyer at al., 1968, for descriptions). Butte Quartz Monzonite adjacent to these veins is altered to advanced argillic, sericitic, and intermediate argillic mineral assemblages (Sales and Meyer, 1948; Meyer and Hemley, 1967). On a deposit scale, Main stage mineralization is zoned from an interior Cu-rich zone, through an intermediate Cu-Zn zone, to a peripheral Mn, Pb, Zn, and Ag zone (Meyer et al., 1968) (Fig. 4L, M).

Fluid Inclusion Petrography

Fluid inclusion assemblages

Interpretation of fluid inclusions in porphyry Cu deposits is difficult because superposition of multiple stages of fracturing, fluid flow, and mineralization obscures timing relationships among vein minerals, alteration minerals, and fluid inclusion populations, also obscuring the source and evolution of hydrothermal fluids. Multiple hydrothermal stages juxtapose fluid inclusions trapped from chemically, physically, and temporally distinct fluids in a single vein. Petrographic studies and SEM-cathodoluminescence imaging were employed to decipher the complex relationships between fluid inclusions and the minerals in which they are trapped (Rusk and Reed, 2002; Rusk, 2003; Rusk et al., 2006).

Petrographic studies and inclusion analyses focused on fluid inclusion assemblages (Goldstein and Reynolds, 1994). A group of inclusions were trapped synchronously and therefore represent a true fluid inclusion assemblage if the inclusions were trapped along the same primary growth zone in quartz, or along the same healed fracture. At Butte, as in most porphyry Cu deposits, it is difficult to identify fluid inclusions in vein quartz that meet the above criteria. In pre-Main stage veins, quartz with euhedral growth zones is rare and fluid inclusions located along primary growth zones in euhedral quartz are extremely rare. The vast majority of fluid inclusions occur in scattered groups and clusters without unambiguous evidence for contemporaneous trapping. Most inclusions measured in this study occur in groups or clusters of inclusions containing similar liquid-to-vapor ratios in a single grain or in several nearby grains of quartz. Where groups or clusters of inclusions exhibit similar heating and freezing behavior, we infer that they were trapped from similar fluids under similar conditions and so have a common origin.

Fluid inclusion types

On the basis of phases present at room temperature, we distinguish six types of fluid inclusions at Butte, classified as types B35, B60, B15H, B85, and B20. In this classification system, the letter "B" denotes "bubble," and the number indicates the average volume percent occupied by the bubble (vapor) in inclusions of that type. The letter "H" refers to the presence of halite as a daughter mineral. B20 fluid inclusions are divided into B20 and $B20_{MS}$, which refers to whether these inclusions occur in pre-Main stage veins or Main stage veins, respectively. Further subdivision based on daughter mineral assemblages or vein types is possible using this classification system, but such subdivisions are not necessary here.

B35 fluid inclusions contain liquid and a vapor bubble that occupies 30 to 50 vol percent of the inclusion and lacks halite daughter minerals at room temperature (Fig. 5A, H, K). These inclusions are typically the shape of negative quartz crystals or rounded rectangles. Approximately 20 percent of B35 inclusions contain an opaque and/or a transparent daughter mineral, and a few contain up to four daughter minerals. The most common daughter mineral is opaque and triangular in cross section, identified by SEM-EDS in many opened inclusions as Cu-Fe sulfide, most likely chalcopyrite (also identified by Roberts, 1975). Transparent daughter minerals (or possibly trapped solids) identified with EDS include K-feldspar, anhydrite, and calcite. Rutile and iron oxide were also identified in B35 fluid inclusions; however, daughter minerals of molybdenite were never identified. No B35 daughter minerals homogenized even when the inclusion was heated past its expected homogenization temperature for several minutes. This suggests that H_2 leaked from the inclusions after entrapment (Mavrogenes and Bodnar, 1994). B35 inclusions were rarely identified as primary along euhedral growth zones of quartz or as secondary or pseudosecondary along healed fractures. Instead, most B35 inclusions are densely scattered across multiple quartz grains or are grouped in clusters in individual quartz grains.

B60 inclusions contain liquid and 50 to 75 vol percent vapor at room temperature and typically have negative crystal shapes or are equant (Fig. 5B). About 15 percent contain one or two opaque daughter minerals, and a few contain one or two transparent daughter minerals. Daughter minerals identified by SEM-EDS include Cu sulfides, Cu-iron sulfides, zinc sulfides, and muscovite. There is a continuous gradient in bubble size between B35 and B60 inclusions; therefore, distinguishing between B35 inclusions and B60 inclusions at room temperature is sometimes difficult. Like B35 inclusions, B60 inclusions are clustered, scattered variably (Fig. 5I, L), and occur less commonly along secondary or pseudosecondary trails.

B15H inclusions contain liquid plus 10 to 20 vol percent vapor plus halite at room temperature (Fig. 5C, F). Rarely, B15H inclusions contain up to five daughter minerals besides halite; however, in contrast to many porphyry Cu deposits (Alumbrera, Bingham, Santa Rita, Red Mountain, and others) most B15H inclusions from Butte contain no other daughter minerals in addition to halite. Also in contrast to other porphyry Cu deposits, B15H inclusions from Butte rarely contain sylvite or any other phase that dissolves upon heating to and beyond the homogenization temperature of halite. Less than 5 percent of B15H inclusions contain a red hexagonal hematite daughter mineral or a tetrahedral opaque chalcopyrite crystal. B15H inclusions are nearly always in quartz that also contains B85 inclusions (Fig. 5C), and a few unambiguous trails of B15H and B85, trapped simultaneously, were recognized. Nonetheless, most trails or clusters contain only one inclusion type or the other. Like the other inclusion types, B15H inclusions are commonly scattered variably in vein and igneous quartz.

B85 inclusions contain more than 75 vol percent vapor at room temperature (Fig. 5C). A few B85 inclusions contain an opaque or a transparent daughter mineral; however, daughter minerals could not be positively identified optically or with SEM-EDS. B85 inclusions are most abundant in quartz that also contains B15H inclusions; however, some are present

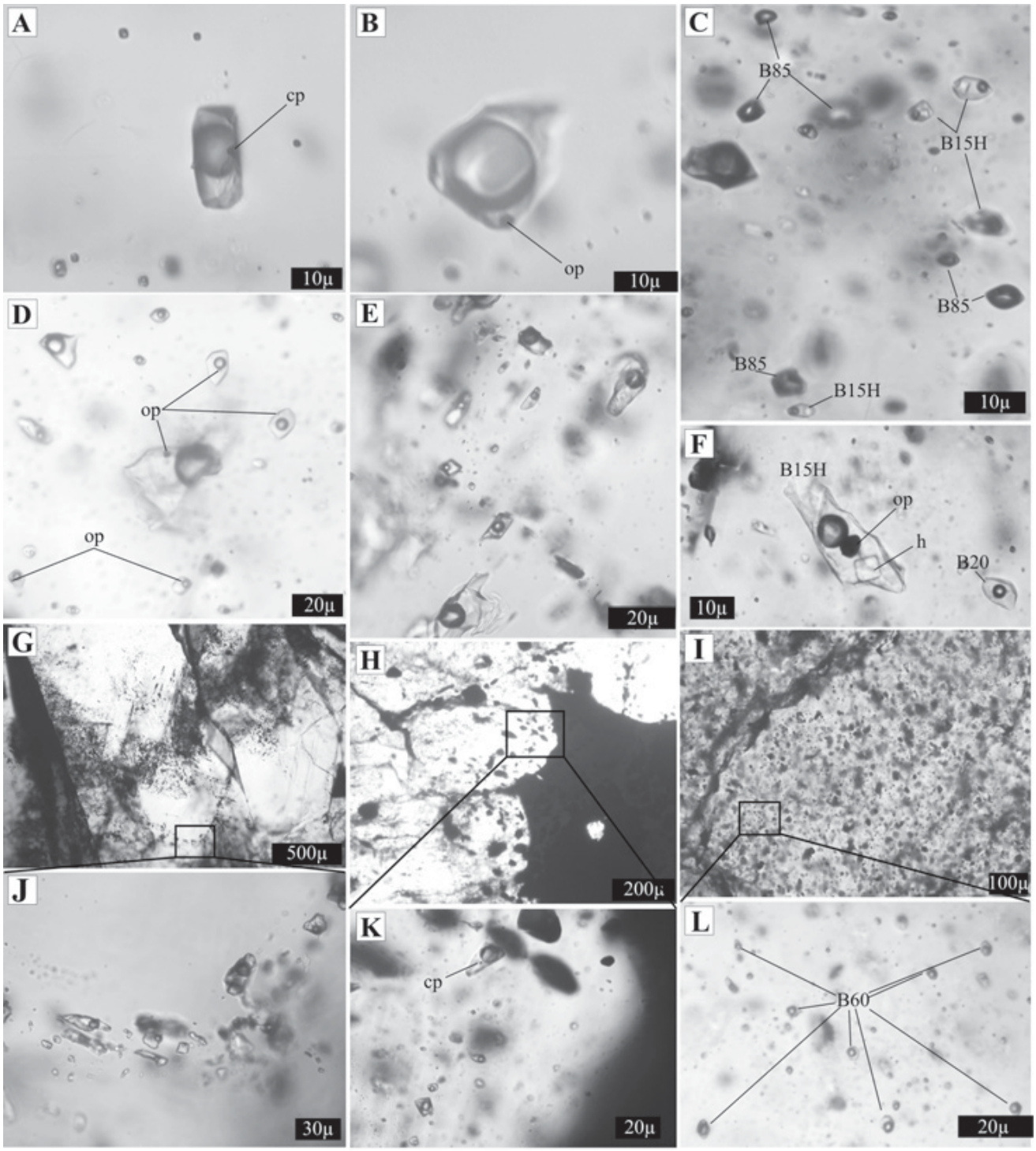

Fig. 5. Transmitted light photomicrographs of Butte fluid inclusions. A) B35 fluid inclusion containing ~35 vol percent bubble and a triangular opaque daughter mineral which is likely chalcopyrite (cp). B) B60 inclusion containing ~60 vol percent bubble and an unidentified opaque daughter mineral (op). C) Vapor-rich B85 fluid inclusions and halite-bearing B15H fluid inclusions. Rarely, brine and vapor inclusions coexist on the same healed fracture, but more commonly the inclusions appear scattered and healed fractures are not obvious. D) B20 fluid inclusions, many containing a single opaque daughter mineral. E) Primary $B20_{MS}$ inclusions trapped along quartz growth zones in a Main stage vein. F) A large B15H inclusion trapped near several high salinity B20 inclusions. G) Primary fluid inclusions trapped along growth zones in euhedral quartz from a Main stage vein. H) Primary B35 fluid inclusions and small chalcopyrite crystals trapped in quartz projecting into chalcopyrite. I) Low-power image of a quartz crystal in a barren quartz vein from deep in the zone of pervasive sericitic alteration. B60 Fluid inclusions are very abundant and are not distributed along primary growth zones or along secondary trails as is typical of inclusions from Butte and many other porphyry Cu deposits. J) Enlargement of G. K) Enlargement of H. L) Enlargement of I.

where B15H inclusions are lacking. B85 inclusions are typically scattered or in clusters within quartz grains.

B20 inclusions contain liquid and 10 to 30 vol percent vapor at room temperature (Fig. 5D). About 10 percent of B20 inclusions in pre-Main stage veins contain one opaque daughter mineral; a few contain up to three opaque or transparent daughter minerals. Equant and rectangular B20 inclusions are commonly scattered thinly and randomly throughout a vein. In deep veins, irregularly shaped B20 inclusions are common in planar trails. These lack daughter minerals and are secondary in origin.

$B20_{MS}$ inclusions are similar in appearance to B20 inclusions, but none was observed to contain opaque daughter minerals, and only a few contain transparent daughter minerals. $B20_{MS}$ inclusions occur as both secondary inclusions along planar trails and primary inclusions trapped along quartz growth zones in Main stage veins (Fig. 5E, G, J).

Deposit-scale distribution of fluid inclusions

The distribution of inclusion types throughout the deposit reflects the processes that led to mineral precipitation and wall-rock alteration. We examined the distribution of fluid inclusion types to determine the relationships between trapped fluids and vein and alteration types, as well as the time and space relationships among various fluids. The estimated abundance of each type of inclusion in 38 samples is shown in Table 2, along with the vein and alteration type, sample location, and the Cu, Mo, and Ag grade of the interval from which the sample came. The general pattern of fluid inclusion distribution relative to alteration zones and vein types can be inferred from Table 2 and is illustrated in Figure 6. Fluid inclusion distribution is similar in both the Pittsmont and Anaconda domes. All stated depths refer to fault-corrected depths beneath the present surface west of the Continental fault. Fluid inclusion abundance estimates have relatively large uncertainties owing to the abundance of inclusions in most samples and the difficulty of estimating bubble size in small inclusions. B60 and B85 inclusions are typically larger than B35 inclusions, and B15H and B20 inclusions are typically smaller. Furthermore, a B35 or B20 inclusion, viewed on end, appears to be a B60 or B85 inclusion, but the reverse is not likely.

B35 inclusions dominate in veins from the deepest samples recovered, from about 1,600 m below the present surface to the bottom of the deepest drilling (~2,600 m), except in the pervasively altered sericitic zone, where B60 inclusions dominate at all drilled depths. At depths greater than 1,600 m, deep, early dark micaceous and barren quartz–quartz-molybdenite veins dominate, and B35 inclusions constitute more than 95 percent of all inclusions. B35 inclusions are far less common in all vein types at depths less than ~1,000 m, where B85 and B60 inclusions dominate and B15H inclusions are common (Fig. 6).

B60 inclusions are rare east of the Continental fault, although a few were identified in a sample where a gray sericitic vein cuts a quartz-molybdenite vein. B60 inclusions

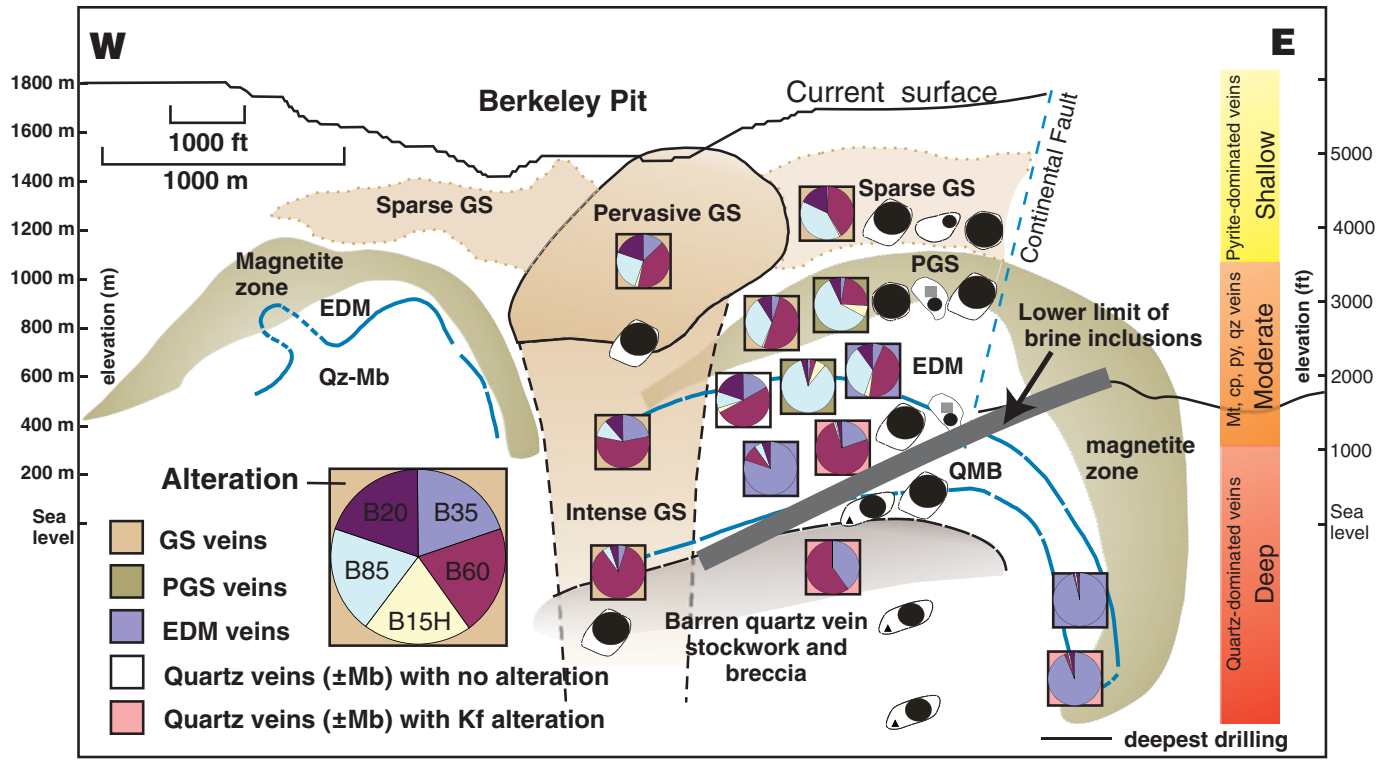

FIG. 6. Deposit-scale distribution of fluid inclusions and vein and alteration types prior to displacement of the Continental fault. Pie graphs show the abundance of each inclusion type estimated in individual samples with different alteration styles from various depths. The lower limit of B15H inclusions is indicated by the thick black line. Below the line, B15H inclusions are absent and B35 and/or B60 inclusions dominate all samples. The distribution of fluid inclusions is represented by schematic diagrams of fluid inclusion types.

TABLE 2. Deposit Scale Distribution of Fluid Inclusion Types Showing the Relative Abundance of Inclusions in 38 Selected Samples

Location	Sample no.	Vein/ alteration type	Depth below surface (m)	Cu grade[1] wt%	Mo grade[1] wt%	Ag grade[1] oz/ton	B35	B60	B15H	B85	B20
East of CF											
Pittsmont	11172-2756	qz/EDM	2148	0.15	0.047	NA	96	1	0	1	2
Pittsmont	bu96mr15	qz/EDM	1300	NA[2]	NA	NA	90	5	0	3	2
Pittsmont	8741-270	bi veinlets	1383	NA	NA	NA	90	5	0	3	2
Pittsmont	11172-3186	qz-mb/kf	2280	0.21	0.055	NA	97	tr	0	tr	3
Pittsmont	11172-4187	qz-mb/kf	2588	0.09	0.030	NA	94	2	0	1	3
Pittsmont	11172-513	qz-mb/kf	1458	0.13	0.041	0.058	97	tr	0	tr	3
West of CF											
Pittsmont	11185-4842	qz/EDM	0	0.34	0.063	0.116	80	10	tr	5	5
Pittsmont	11135-3618	qz/EDM	0	0.52	0.040	0.052	7	45	3	35	10
Pittsmont	11185-3448	qz/EDM	0	0.29	0.040	0.095	9	40	1	45	5
Anaconda	10772-5	mt-qz/EDM	741	(0.30)[3]	(0.005)	NA	tr	tr	2	90	8
Pittsmont	11185-1797	qz-mt/PGS	0	0.27	0.008	0.052	5	10	2	80	3
Anaconda	10961-766	mt-qz/PGS	621	0.26	0.007	0.092	3	23	7	60	7
Anaconda	10530-407	mt-cp-py/PGS	682	0.36	(0.01)	NA	2	35	5	53	5
Pittsmont	11185-2091	mt-cp-qz/PGS	0	0.35	0.007	0.073	2	3	6	85	4
Anaconda	10893-34	mt-cp-py/PGS	447	0.30	0.006	0.041	3	6	6	80	5
Pittsmont	11169-5286	qz/kf	0	0.25	0.035	0.180	97	tr	0	tr	3
Pittsmont	11169-5061	qz-mb/kf	0	0.13	0.060	0.079	50	40	1	3	6
Pittsmont	11169-4909	qz/kf	0	0.12	0.047	0.065	40	60	0	tr	tr
Pittsmont	11135-5149	qz/kf	0	0.11	0.041	0.017	32	60	tr	5	3
Pittsmont	11135-4947	qz/kf	0	0.09	0.065	0.003	12	80	tr	5	3
Pittsmont	11135-4326	qz/kf	0	0.32	0.045	0.024	15	80	tr	1	4
Pittsmont	11135-3872	qz-mb/kf	0	0.55	0.026	0.662	17	50	3	10	20
Pittsmont	11135-3618	qz-mb/kf	0	0.52	0.040	0.052	15	78	2	1	4
Pittsmont	11166-5862	qz-mb/kf	0	0.18	0.031	0.092	70	25	tr	tr	5
Pittsmont	11185-4386	qz-mb/kf	0	0.26	0.064	0.070	20	75	1	1	3
Pervasive GS zone											
Central GS zone	10969-1849	py-qz/pervasive GS	0	0.16	0.002	0.031	13	40	2	25	20
Central GS zone	11052-5705	py-qz/pervasive GS	0	0.17	0.041	0.013	30	30	tr	10	30
Central GS zone	11052-6769	py-qz/pervasive GS	0	0.03	0.009	0.001	20	50	tr	10	10
Central GS zone	11052-7023	qz/pervasive GS	0	0.02	0.007	0.000	5	85	0	5	5
Shallow GS											
Pittsmont	11148-1141	py-qz/GS	0	0.11	<.001	0.036	1	40	1	40	18
Pittsmont	11148-1302	py-qz/GS	0	0.12	<.001	0.035	1	50	1	35	13
Pittsmont	11169-1306	py-qz/GS	0	0.15	<.001	0.018	5	50	1	35	9
Anaconda	9201	py-qz/GS	1022	NA	NA	NA	20	30	tr	25	25
Anaconda	10835-10	py-qz/GS	1113	NA	(0.01)	NA	10	50	5	20	15
Main stage											
Central zone	CZ-1	en-py-cv	NA	NA	NA	NA	0	0	0	0	100
Central zone	10555-1	en-py-cv	115	NA	NA	NA	0	0	0	0	100
Periphery	4927	rc-qz	120	NA	NA	NA	0	0	0	0	100
Periphery	11172-3658	rc-py-qz	1126	0.29	0.061	0.029	0	0	0	0	100

Abbreviations as in Table 1

[1] Average Cu, Mo, and Ag grade for the 20-m interval in which the sample lies

[2] NA indicates that the data is not available

[3] Numbers in parentheses indicate approximate grades

dominate in gray sericitic veins from all locations in the deposit. B60 inclusions are also abundant in early dark micaceous and barren quartz–quartz-molybdenite veins from depths between ~1,200 and 1,600 m. In many of these veins, most inclusions range from B35 to B60, and B15H and B85 inclusions are present but rare. B60 inclusions are present but are not dominant in pale-green sericitic veins at depths less than 900 m (Fig. 6).

B15H inclusions are rare at depths greater than ~1,600 m, where B35 inclusions dominate. Conversely, B15H inclusions are more common in veins from depths less than ~1,000 m, where B35 inclusions are rare. B15H inclusions are more common in magnetite-chalcopyrite-pyrite-bearing veins with pale-green sericitic alteration envelopes, and in early dark micaceous veins from depths shallower than ~1,200 m, than in any other vein type or location (Fig. 6). The samples with the largest proportions of B15H inclusions are magnetite-dominated pale-green sericitic veins. Even so, these magnetite-dominated veins, from both the Anaconda and the Pittsmont domes, contain only ~5 to 8 percent B15H inclusions, with the majority of the inclusions being B85s and B60s. B15H inclusions are present in all pre-Main stage vein types shallower than ~1,400 m, but they are not present in any Main stage vein from any depth. Most B15H inclusions

occur in close proximity to B85 inclusions, and in a few samples, vapor-rich and brine inclusions occupy the same healed fracture.

B85 inclusions are most abundant in veins from less than ~900 m in both the Anaconda and Pittsmont domes and they are rare in veins from depths greater than 1,200 m. They are the dominant inclusion type in most pale-green sericitic veins and are common in gray sericitic veins. Most occur in the same veins as B15H inclusions, and assemblages containing only B85 or only B15H inclusions were identified.

B20 inclusions occur in all vein types from all depths in the deposit but do not dominate in any pre-Main stage vein type. East of the Continental fault, they occur only along secondary trails, whereas west of the Continental fault, they are more abundant in clusters and scattered throughout the sample. They are most abundant in gray sericitic veins but are subordinate in abundance to B60 and B85 inclusions. Cathodoluminescence textures indicate that many B20 inclusions on secondary trails in pre-Main stage veins are trapped along healed fractures of apparent Main stage origin (Rusk et al., 2006).

$B20_{MS}$ inclusions are both primary and secondary in quartz, fluorite, sphalerite, and rhodochrosite in Main stage veins. No other inclusion type was observed in Main stage veins. Owing to the similar phase proportions of B20 and $B20_{MS}$ inclusions, it is impossible to determine at room temperature whether B20 inclusions in pre-Main stage veins are from pre-Main stage or Main stage mineralization.

Physical and Chemical Properties of Inclusions

CO_2 content of fluid inclusions

We have identified substantial amounts of CO_2 in B35, B60, B85, and $B20_{MS}$ inclusions, but none in B20 or B15H inclusions. Liquid CO_2 at room temperature was optically identified in only two B35 inclusions from deep in the deposit. Measured melting temperatures of –56.6° ± 0.1°C in these two inclusions and in three others in which a solid phase formed upon cooling indicate that CO_2 is the predominant gas. In inclusions with no visible CO_2, cooling to –30° to –35°C formed clathrate in most B35, B60, and B85 inclusions. The presence of CO_2 in $B20_{MS}$ inclusions also was indicated by the expansion of bubbles upon crushing in oil (Roedder, 1984). Raman spectroscopy confirmed the presence of CO_2 in both B35 and B60 inclusions (the only types analyzed) in seven samples and that dissolved gases other than CO_2 are minor in these inclusions. The 19 inclusions analyzed by Raman spectroscopy contain 3.1 to 7.8 mol percent CO_2 (Fig. 7), with no significant difference in CO_2 content between B35 and B60 inclusions.

Because the clathrate structure includes H_2O but excludes NaCl, ice-melting temperature in the presence of clathrate results in an overestimation of salinity by a factor of up to three (Collins, 1979). Accurate estimates of salinity can be determined based on clathrate melting temperatures if the inclusion contains CO_2 liquid, CO_2 vapor, and aqueous fluid of unknown salinity at the temperature of clathrate melting ($Tm_{Clathrate}$) (Larson, 1955; Takenouchi and Kennedy, 1965; Chen, 1972; Bozzo et al., 1975; and Collins, 1979). If no CO_2 liquid is present at room temperature, but it condenses upon cooling of the inclusion, then the homogenization temperature of CO_2 in the metastable absence of clathrate constrains the internal pressure of the fluid inclusion, so that the salinity can be constrained (Diamond, 1992). With few exceptions, inclusions from Butte do not contain liquid CO_2 at room temperature, nor do they condense liquid CO_2 upon cooling. Such behavior complicates the determination of salinity based on microthermometric measurements.

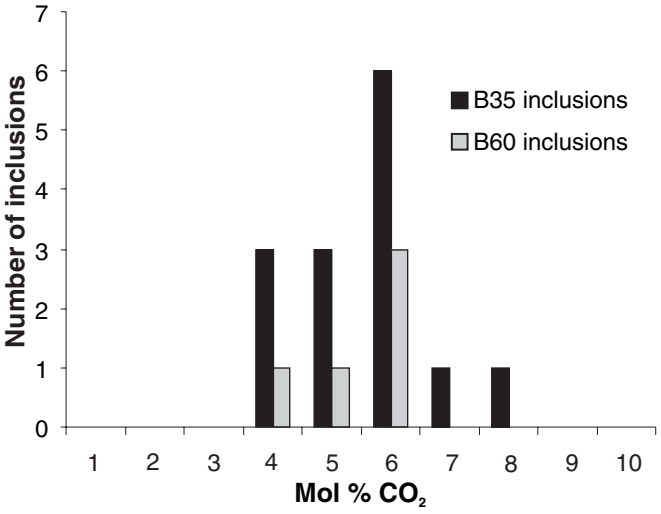

FIG. 7. Histogram showing CO_2 content of 19 B35 and B60 inclusions analyzed by Raman spectroscopy.

Dubussey et al. (1992) developed a technique to determine the bulk properties of fluid inclusions that form clathrate upon cooling but contain no liquid CO_2. The method of Debussey et al. (1992) was modified slightly by Bakker et al. (1996) and incorporated into the computer program ICE (Bakker, 1997), which calculates salinity, density, and CO_2 content of inclusions based on ice-melting temperatures, clathrate-dissolution temperatures, and an estimate of bubble volume. Precise estimates of bubble volume are difficult because of the variability of inclusion shape and orientation (Parry, 1986; Diamond, 1994; Bakker et al., 1996). Errors in estimating the bubble volume have a large effect on calculated density (and therefore isochore slopes), and much smaller effects on CO_2 content and salinity (compare Fig. 8A-C). Salinities, densities, and CO_2 contents were calculated using ICE for B35, B60, and B85 inclusions.

Estimates of the bulk properties of fluid inclusions are possible only where both Tm_{ICE} and $Tm_{Clathrate}$ are measured in the same inclusion, which accounts for only about 10 percent of all clathrate-bearing inclusions measured. Melting temperatures of ice and clathrate were similar among all inclusions, whether both or just one of the phase changes—were observed. We infer, therefore, that bulk properties of inclusions in which only one of the phase changes was observed are similar to the bulk properties of inclusions in which both phase changes were observed.

For 98 of the 106 inclusions in which both phase changes were observed, the CO_2 contents calculated by ICE fall within the range measured with the Raman microprobe. Most CO_2 contents predicted by ICE are within 1 mol percent of the values measured by Raman on the same inclusion (Fig. 9).

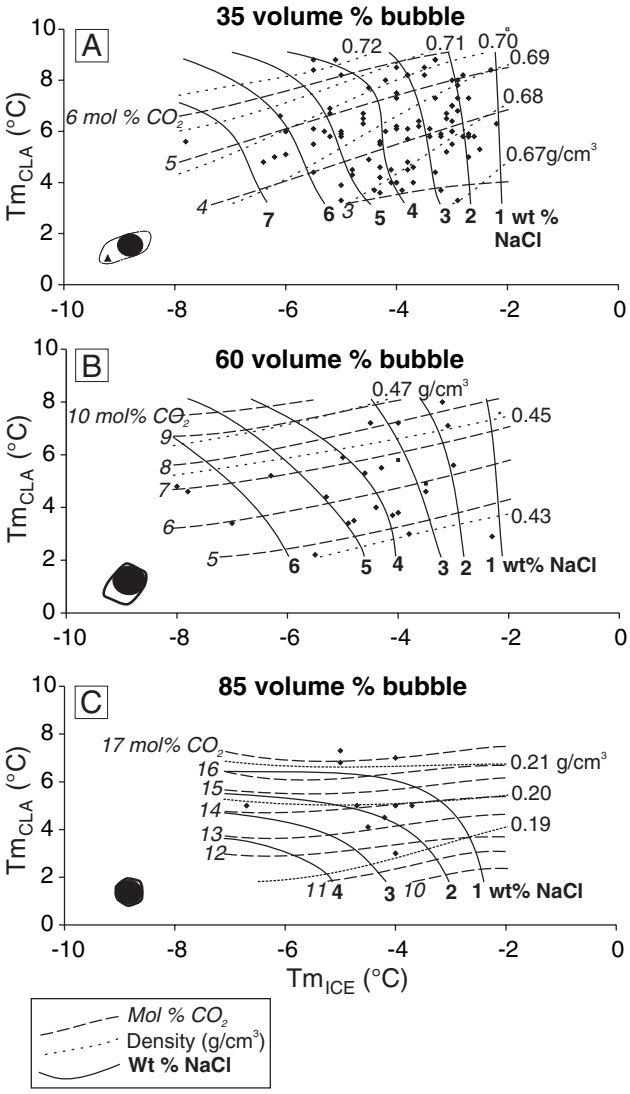

FIG. 8. Temperatures of ice melting (Tm_{ICE}) and clathrate melting ($Tm_{Clathrate}$) for A) B35 inclusions, B) B60 inclusions, and C) B85 inclusions. Based on measured melting temperatures of ice and clathrate, and visual estimation of bubble volume in the inclusion, bulk inclusion properties were calculated using the program ICE (Bakker, 1997). Filled diamonds represent all inclusions in which both ice and clathrate were observed to melt (except in B85 inclusions; see text). Diagrams are contoured for salinity, CO_2 content, and bulk density, assuming 35, 60, and 85 vol percent bubble (see text for isopleth source). Comparison of the three graphs shows the effect of fluid inclusion bubble volume on calculation of bulk properties.

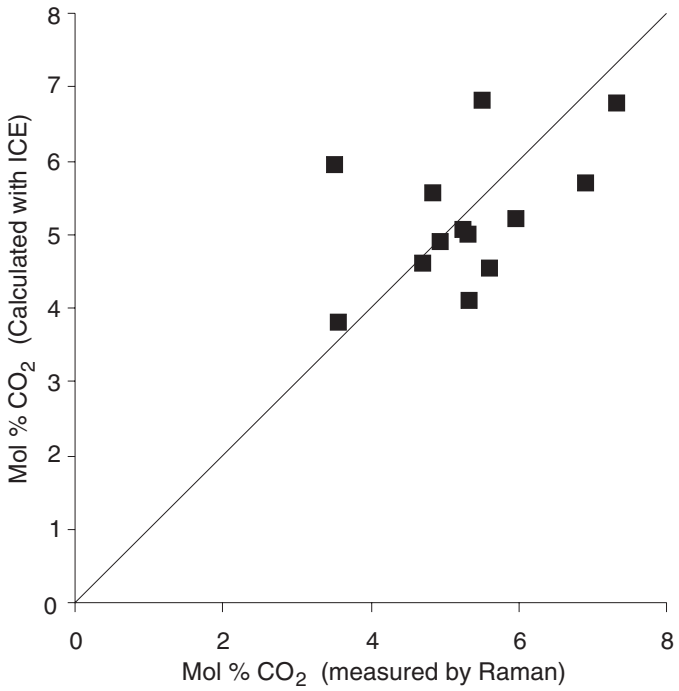

FIG. 9. Comparison of CO_2 content calculated from microthermometric data using the program ICE, and CO_2 content measured by Raman spectrometry in the same inclusion (see text). The diagonal shows a 1:1 correlation. Most calculated CO_2 contents fall within 1 mol percent of measured CO_2 contents.

Microthermometry

B35 inclusions: Among B35 inclusions, 63 percent were observed to form clathrate upon cooling. Calculated CO_2 contents of clathrate-bearing inclusions are 3 to 7 mol percent CO_2 (Fig. 8).We assume that nonclathrate-bearing B35 inclusions contain ~3 mol percent CO_2. Clathrate in B35 inclusions melts between 3° and 9°C (Fig. 10). In these same inclusions, ice melts in the presence of clathrate between –2° and –8°C, corresponding to salinities in the range of 1 to 8 wt percent NaCl equiv, with 75 percent having salinities between 2 and 5 wt percent NaCl equiv (Figs. 10–12; Table 3). Salinities are between 0 and 6 wt percent NaCl equiv for nonclathrate-forming B35 inclusions, assuming 3 mol percent CO_2. Salinities calculated in the H_2O-CO_2-NaCl system by the program ICE are about half of what is predicted in the H_2O-NaCl system based only on melting temperatures of ice, which indicates that the recognition of clathrate in B35 inclusions is important for accurate salinity determinations. Densities of B35 fluid inclusions in which both Tm_{ICE} and $Tm_{Clathrate}$ were measured are between 0.67 and 0.72 g/cm^3, with an average of 0.69 g/cm^3 (Fig. 8). However, because the calculated densities depend on estimated bubble size, which varies among inclusions categorized as B35 inclusions, densities from 0.63 to 0.73 g/cm^3 are likely.

All B35 inclusions homogenize to liquid between 300° and 400°C, with a mean of 349°C; 88 percent homogenize between 330° and 370°C (Fig. 10). Inclusions within individual clusters typically homogenize within 5° to 10° of one another.

B60 inclusions: Most B60 inclusions form clathrate upon cooling. Clathrate melting temperatures range from 2° to 8°C. Tm_{ICE} in the same inclusions ranges from –2° to –8°C (Fig. 10), corresponding to salinities of 1 to 8 wt percent NaCl equiv with 74 percent having salinities between 1 and 5 wt percent NaCl equiv (Figs. 10–12; Table 3). Calculated CO_2 contents range from 4 to 9 mol percent CO_2, and calculated densities range from 0.43 to 0.49 g/cm^3 (Fig. 8). Actual densities of B60 inclusions range from near 0.4 to 0.55g/cm^3 for inclusions with bubbles slightly more or less than 60 vol percent (compare Fig. 8A-C).

B60 inclusions homogenize to liquid, to vapor, and by critical behavior between 356° and 452°C (avg of 384°C: Fig. 10 and Table 3). An entire cluster of B60 inclusions may

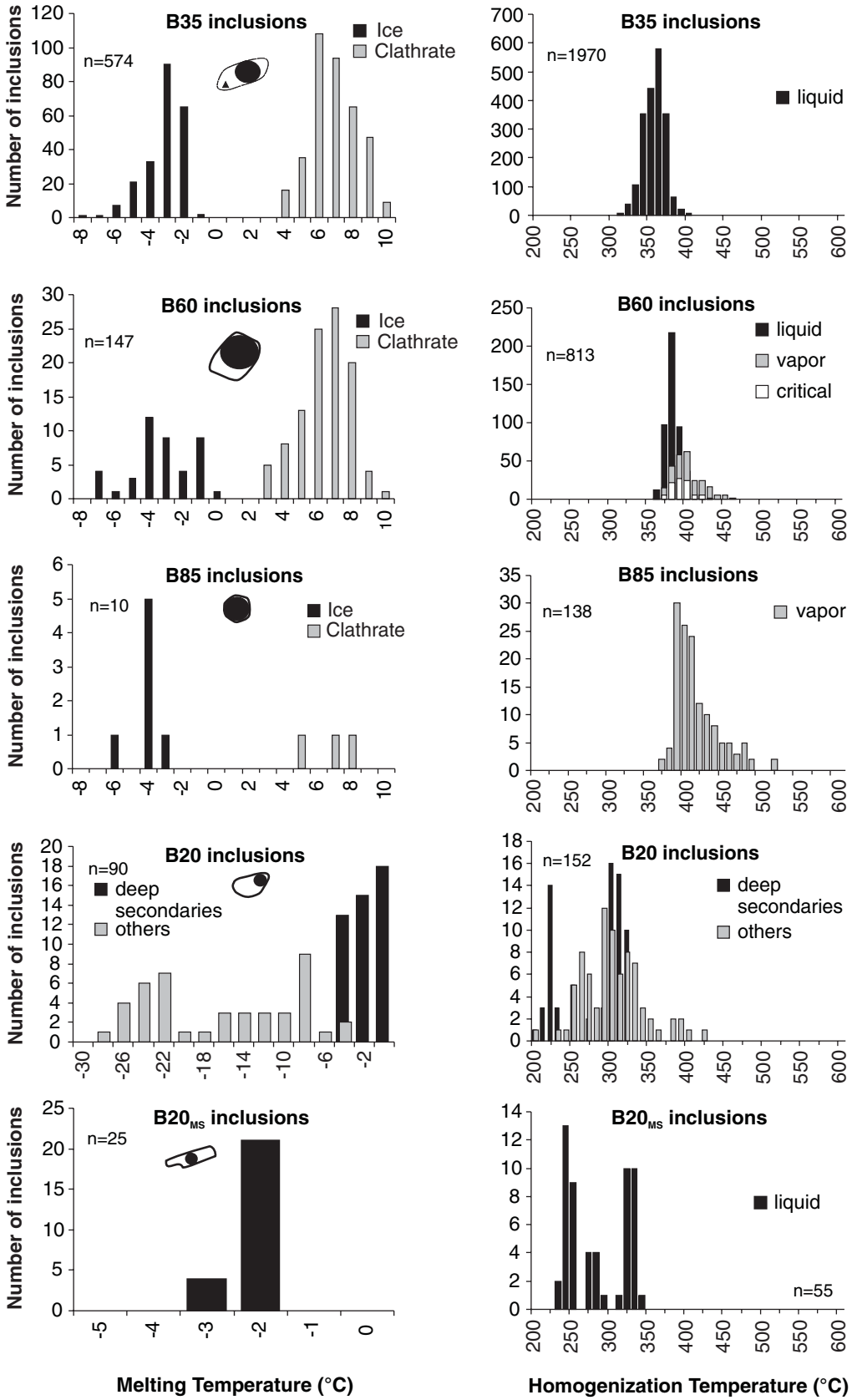

FIG. 10. Histograms showing melting temperatures of ice and clathrate in ~700 B35, B60, B85, B20, and $B20_{MS}$ inclusions and homogenization temperatures to liquid, vapor, or by critical behavior of over 3,000 B35, B60, B85, B20, and $B20_{MS}$ inclusions. These results are compiled from microthermometric measurements of approximately 50 samples.

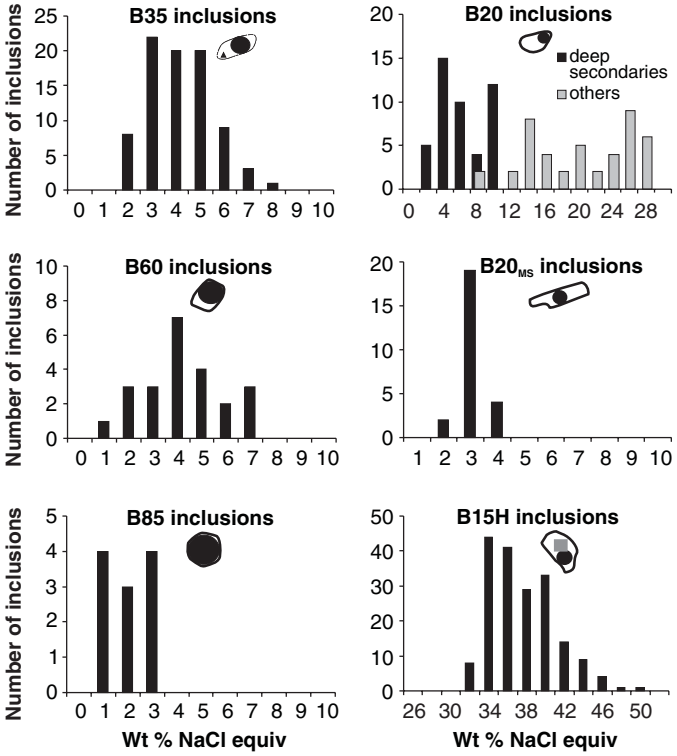

FIG. 11. Histograms showing calculated salinity of all inclusion types. For B35 and B60 inclusions, salinities are only shown for inclusions where both clathrate- and ice-melting temperatures were observed in single fluid inclusions, which accounts for only about 10 percent of all inclusions measured. The narrow range of ice- and clathrate-melting temperatures measured indicates that salinities are likely similar for inclusions where only one of these phase changes was observed.

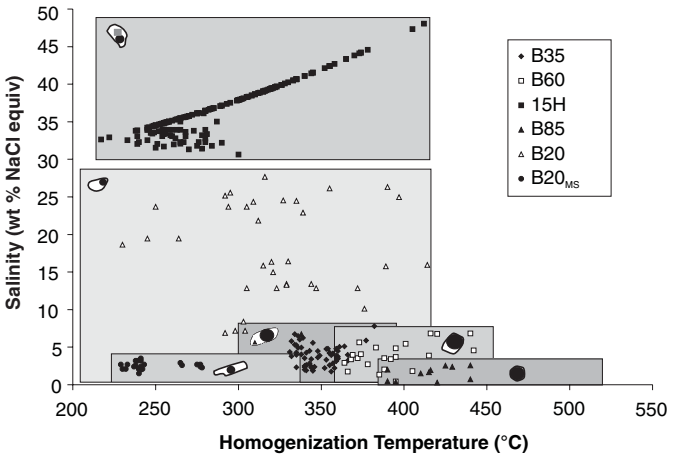

FIG. 12. Homogenization temperature versus salinity of individual inclusions from all inclusion types in which both measurements were made. Boxed, shaded regions show the entire range of salinities and homogenization temperatures measured for each inclusion type. Unlike many studies of porphyry deposits, there are no significant gaps in salinity or homogenization temperature where no inclusions were measured.

homogenize to liquid, to vapor, or by near-critical behavior, but more commonly, all three behaviors of homogenization are observed in a single cluster of inclusions. In inclusions that homogenize by critical behavior, the bubble maintains a constant size upon heating, until the meniscus that separates the vapor from the liquid fades away over a range of about 5°C. Many B60 inclusions homogenize with near-critical behavior, either to liquid or to vapor. In each case, little change is observed in bubble size until within 5° to 15°C of homogenization, at

TABLE 3. Microthermometric Properties of Fluid Inclusions

Inclusion type	Homogenization range (°C)	Average homogenization temperature (°C)	Salinity (wt % NaCl equiv) [1]	Mol % CO_2 [2]	Density g/cm^3	Deposit-scale distribution
B35 n = 2544	300-400 88% between 330-370	Liquid = 349	1-8 avg = 4	3–8	0.63–0.72	Most abundant in deep BQ/QMB and deep EDM veins
B60 n = 960	356-452 86% between 360-400	Liquid = 377 Critical = 388 Vapor = 396	1-7 avg = 4	3–9	0.42–0.55	In all vein types at moderate to shallow depths; most abundant in and around GS veins
B15H n = 187	175-412 72% homogenize by halite dissolution	Liquid = 238 Halite = 278	30-48 avg = 38	0	1.1–1.2	Few deeper than ~1400 m; in all vein types at moderate to shallow depths; commonly near B85 inclusions
B85 n = 148	370-520	Vapor = 413	0-3 avg = 1.5	10–20	<0.1–0.21	In all types at moderate to shallow depths; few deeper than ~1400 m; present in some veins where B15H inclusions are lacking
B20 n = 242	195-400	Liquid = 285	1-28 avg = variable multiple origins	0	variable	Most abundant in GS veins; not dominant in any pre-Main stage vein type
B20(MS) n = 90	140-340	Liquid = 277	1.0- 3.5 avg = 2.6	<2	0.9	Primary and secondary in Main stage veins

[1] Salinities are given in wt percent NaCl equivalent on a H_2O-NaCl-only basis
[2] CO_2 contents are in mol percent on CO_2-H_2O-only basis
[3] Abbreviations: n = number of inclusions analyzed, avg = average, other abbreviations as in Table 1

which point the bubble fades and shrinks or expands rapidly at the temperature of near-critical homogenization. In these inclusions, little undercooling is necessary to renucleate the bubble after homogenization. Most inclusions homogenize to vapor at a higher temperature than nearby inclusions that homogenize to liquid or by critical behavior; however, the ranges of all three homogenization behaviors overlap (Fig. 10). Like B35 inclusions, inclusions within clusters typically homogenize within 10° of one another.

B15H inclusions: Halite dissolution temperatures range from 175° to 412° (Table 3). Of all B15H inclusions, 72 percent homogenize by halite dissolution above the temperature of L-V homogenization, whereas the rest homogenize by L-V homogenization after halite dissolution (Fig. 13). Halite dissolution occurs at temperatures up to 172°C higher than bubble homogenization in some groups of inclusions.

In recent studies of several porphyry Cu deposits, several distinct types of halite-saturated fluid inclusions have been distinguished based on daughter minerals (cf. Alumbrera: Ulrich et al., 2001) or homogenization behavior and distribution within individual veins (Bingham: Redmond et al., 2004; Landtwing et al., 2005). At Butte, however, no distinct populations of halite-bearing inclusions were identified. In different assemblages of B15H inclusions within a single sample, halite dissolution temperatures range over 160°C, equivalent to a range of about 16 wt percent NaCl equiv. This range is only slightly less than the salinity range of all halite-bearing fluids measured in all samples. Within some clusters of B15H inclusions, homogenization temperatures of bubble or halite differ by as much as 40°C among inclusions. This may result from post-trapping modifications or entrapment of heterogeneous fluids (see below).

B85 inclusions: Melting temperatures of ice and clathrate in B85 inclusions are difficult to observe because of the large bubble size, and they were only observed in a few inclusions.

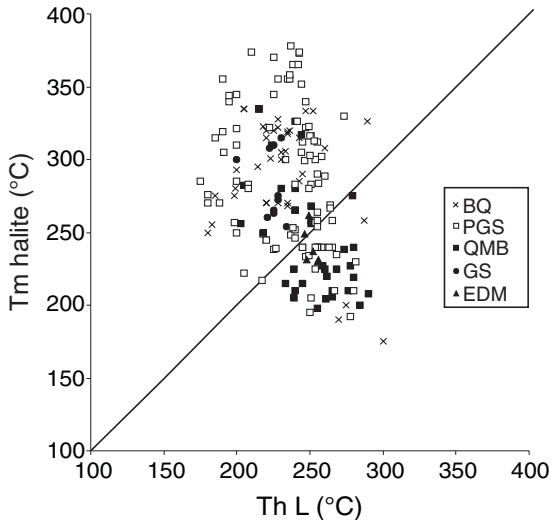

FIG. 13. Temperature of bubble homogenization versus temperature of halite dissolution in 187 B15H inclusions. The diagonal line is the line along which both halite and bubble homogenize at the same temperature. Of the B15H inclusions, 72 percent plot above this line, indicating that halite dissolves after bubble homogenization. Such homogenization behavior indicates that these inclusions were not trapped on the L-V curve, but must have been trapped at some greater pressure.

The formation of clathrate upon cooling in some B85 inclusions indicates the presence of CO_2, but both ice- and clathrate-melting temperatures were never observed in a single inclusion. If we assume for B85 inclusions that the range of melting temperatures of ice and clathrate is limited as shown for B35 and B60 inclusions, then salinities can be estimated based on the Tm_{ICE} and $Tm_{Clathrate}$ from different B85 inclusions. Figure 8C shows the range of salinities, densities, and CO_2 contents calculated with ICE for inclusions containing 85 vol percent vapor. Salinities of B85 inclusions are estimated between 0 and 3 wt percent NaCl equiv (Figs. 10-12; Table 3) and calculated CO_2 contents are as high as 18 mol percent. The CO_2 content of B85 inclusions containing more than 85 vol percent bubble is more than 18 mol percent.

All B85 inclusions homogenize to vapor between 370° and 520°C (Fig. 10). Homogenization temperature in B85 inclusions cannot be precisely determined and is likely to be underestimated by as much as 100°C (Bodnar et al., 1985; Sterner, 1992), owing to the difficulty in observing the disappearance of the last bit of aqueous fluid. True homogenization temperatures are inferred to be between 400° and 600°C for most B85 inclusions.

B20 inclusions: B20 inclusions occur both as scattered clusters of inclusions and as secondary inclusions on planar trails in pre-Main stage veins. Salinities in scattered B20 inclusions range widely between 6 and 28 wt percent NaCl equiv (Figs. 10–12; Table 3) and first-melting temperatures range between –23° and –48°C, indicating a presence of dissolved salts besides NaCl and KCl (Sterner and Bodnar, 1984). Homogenization temperatures of scattered B20 inclusions also range widely between 195° and 420°C (Fig. 10). Individual groups of B20 inclusions typically have a wide range of salinities and homogenization temperatures. The common occurrence of high salinity B20 inclusions near B15H inclusions suggests that in some cases the two types are related but that B20 samples are slightly less saline as a result of postentrapment modifications such as necking or leaking.

Secondary B20 inclusions located in planar trails in deep veins contain less than 10 wt percent NaCl equiv and no daughter minerals. Compared to the scattered B20 samples, these inclusions homogenize over a more narrow range of 200° to 330°C, and inclusions along a single trail homogenize within ~20° of each other. The differences in distribution, daughter minerals, salinity, and homogenization behavior indicate that B20 inclusions trapped on planar trails are of a different origin than scattered B20 inclusions.

$B20_{MS}$ inclusions: Ice-melting temperatures in $B20_{MS}$ inclusions range from –0.4° to –3.3°C (Fig. 10). Roedder (1971) reports similar results for similar inclusions in sphalerite and quartz in a Main stage sample from Butte. In the pure H_2O-NaCl system, such melting temperatures correspond to salinities of 0.7 to 6 wt percent NaCl equiv. Emission of bubbles from several samples crushed in oil indicates that a noncondensable gas is present, likely CO_2. Clathrate was never observed in $B20_{MS}$ inclusions, indicating that these inclusions contain less than about 2 mol percent CO_2 (Rosso and Bodnar, 1995). Salinities are estimated to be <0.5 to 3.5 wt percent NaCl equiv, based on the estimated presence of 1 mol percent CO_2 (Figs. 11, 12; Table 3). $B20_{MS}$ inclusions homogenize to liquid between 230° and 340°C (Fig. 10), with all inclusions

within a fluid inclusion assemblage homogenizing within 10°C of each other. These results agree with those of Miller (2004), who reports fluid salinities between 0 and 6 wt percent NaCl equiv and homogenization temperatures between 220° and 350°C in fluid inclusions from 12 Main stage veins.

Interpretation of Fluid Inclusions

Magmatic origin of low salinity fluids

Low salinity B35 inclusions occur primarily in barren quartz–quartz-molybdenite and early dark micaceous veins from the deepest samples recovered (1,400–2,600 m below present surface), where K-silicate alteration dominates. Oxygen and hydrogen isotopes in micas (Zhang, 2000) suggest that K-silicate alteration in this region was produced by magmatic fluids. The presence of anhydrite and plagioclase in these deep veins and in their alteration envelopes indicates that overprinting from later, cooler hydrothermal fluids, which would dissolve anhydrite and convert plagioclase to sericite or clays, was minimal. In these deep, quartz-rich veins, B35 inclusions account for 95 percent of inclusions in both vein and Butte Quartz Monzonite quartz. Where overprinting by later pyrite veins occurs in deep samples, B35 inclusions are stretched and modified, indicating that they predate such overprinting. Based on these observations, we infer that B35 inclusions trapped the magmatic fluids responsible for the formation of deep, quartz-rich veins (± molybdenite, ±chalcopyrite) with K-feldspar and biotitic alteration.

B35 inclusions dominate in deep, quartz-rich veins but are far less common at shallower levels in the deposit. In five deep drill holes, we identified a transition zone below which B35 inclusions dominate and no B15H inclusions are present and above which B60 and B85 inclusions dominate and B15H inclusions are present (Fig. 6). Based on the distribution of these inclusions and the evidence indicating that the veins in which these inclusions were trapped from magmatic fluids at high temperatures with little overprinting from later, cooler fluids, we conclude that B35 inclusions trapped a single-phase aqueous fluid of magmatic origin at pressures and temperatures above the solvus of the fluid. These interpretations are consistent with those of Roberts (1975).

Salinity and CO_2 content in B35 and B60 fluid inclusions are similar; however, B60 inclusions occur mostly at shallower depths than B35 inclusions. The main difference between the two inclusion types is that B60 inclusions have larger vapor bubbles and homogenize at higher temperatures, indicating that B60 inclusions are of lower density than B35 inclusions. The similarity in salinity and CO_2 content of the two and the dominance of B35 and B60 inclusions in samples with mineral oxygen and hydrogen isotope compositions, indicating magmatic fluid-derived alteration (Zhang et al., 1999, Zhang, 2000), suggest that fluids trapped in B60 inclusions are also derived from magmatic fluids. B60 inclusions trapped fluids similar in origin and bulk composition to B35 inclusions but B60 inclusions were trapped at lower pressure and, in some cases, lower temperature (see below) than B35 inclusions.

Fluid immiscibility

Unmixing of supercritical H_2O-NaCl fluids into a high-density brine and a low salinity, low-density vapor has been recognized in many geologic environments (Pichavant et al., 1982, and references therein; Bischoff and Pitzer, 1985) and the position of the solvus, defining the region of immiscibility in the H_2O-NaCl system has been determined experimentally (Sourirajan and Kennedy, 1962; Urusova, 1975; Bodnar et al., 1985; Bischoff and Pitzer, 1989). Fluid inclusion evidence for fluid immiscibility is characteristic of porphyry Cu deposits (Roedder, 1971; Nash, 1976; Roedder, 1984; Bodnar, 1995), and metal and sulfide zoning patterns in these deposits may be a result of the partitioning of metals and other species between vapor and hypersaline liquid (cf. Heinrich et al., 1999; Audétat et al., 2000). Density and compositional differences between the hypersaline and low-density fluids would affect the physical and chemical behavior of these fluids in fractures, in turn affecting the distribution of the precipitated minerals.

Although the deposit-scale distribution of B15H inclusions described above strongly suggests that B15H fluids were generated by unmixing of a parental low salinity magmatic fluid similar to fluids trapped in B35 inclusions, homogenization occurs by halite dissolution after bubble disappearance in 72 percent of B15H inclusions measured. Such homogenization behavior is relatively common in B15H inclusions in magmatic-hydrothermal ore deposits (Dilles and Einaudi, 1992; Cline and Bodnar, 1994; Wang et al., 1999; Brathwaite et al., 2001; Ulrich et al., 2001; Wanhainen et al., 2003; Goldfarb et al., 2004; Bouzari and Clark, 2006) and may result from high trapping pressures (Becker et al., in review). However, at Butte, halite homogenization at temperatures well above homogenization of the bubble in B15H inclusions yields unreasonably high trapping temperatures, suggesting that postentrapment modification occurred.

Bodnar (1994) experimentally determined the liquidus and the isochore slopes for a 40 wt percent NaCl-H_2O solution. We have applied these data to the 36 halite-saturated inclusions from Butte with calculated salinities between 38 and 40 wt percent NaCl equiv (Fig. 14). Using the minimum slope of isochores in the liquid + halite field for a 40 wt percent NaCl

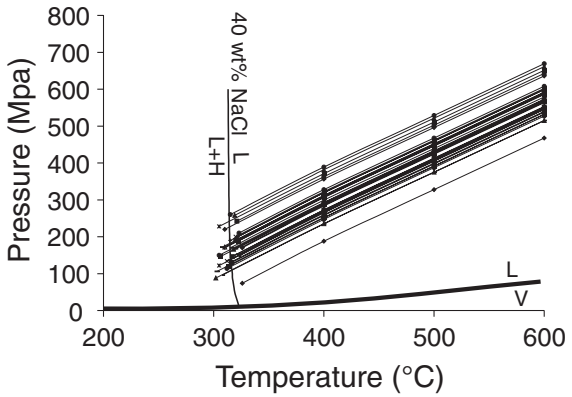

FIG. 14. Isochores of B15H inclusions containing nearly 40 wt percent NaCl. Slopes of these isochores are the experimentally derived minima (Bodnar, 1994). Isochores show that the minimum pressures at which the B15H inclusions were trapped, at the temperature of halite dissolution, is between 70 and 240 MPa. At geologically reasonable temperatures of 500° to 600°C, isochores predict trapping pressures between 450 and 600 MPa. Such pressures are unlikely in this environment and are interpreted to result from post-trapping modification (see text).

solution (2 MPa/°C: Bodnar, 1994), the homogenization behavior of these inclusions corresponds to minimum trapping pressures of 74 to 260 MPa at the temperature of halite dissolution of about 310°C (Fig. 11). Geologic, thermodynamic, and fluid inclusion evidence suggests that these fluids unmixed at temperatures between 400° and 600°C (Reed and Rusk, 2001; Field et al., 2005; this study, see below). Pressure corrections in the liquid field along a minimum estimated isochore slope of 1.4 MPa/°C (Bodnar, 1994) indicate trapping pressures between 200 and 400 MPa at 400°C for these inclusions and pressures greater than 600 MPa at 600°C (Fig. 14). Such pressure-temperature combinations are unlikely in this geologic environment. We therefore conclude that the microthermometry for a majority of measured B15H inclusions yields unreasonable conditions of trapping.

These results suggest that either B15H inclusions trapped an inhomogeneous mixture of multiple fluids or the inclusions have been modified significantly since the time of trapping. Petrographic evidence for inhomogeneous trapping, leaking, or necking was identified in a few samples, but these inclusions were avoided during microthermometry. Modifications of B15H inclusions may have occurred by necking of the vapor phase away from the rest of the fluid or by inclusion migration and water loss as discussed by Audétat and Günther (1999). It is also possible that inclusion stretching during microthermometric heating caused spurious results. To minimize this effect, only one assemblage of B15H inclusions was analyzed by microthermometry in each fluid inclusion chip.

Regardless of the cause for the microthermometric behavior, the deposit-scale distribution of B35, B85, and B15H inclusions indicates that B15H and B85 inclusions were generated by unmixing of B35 fluids and that both brine and vapor were involved, to some extent, in the formation of all pre-Main stage vein types at depths shallower than ~1,400 m (cf. Rusk et al., 2004).

Pressure and temperature of vein formation

Deep, early dark micaceous and barren quartz–quartz-molybdenite veins: The deepest veins studied are quartz-dominated early dark micaceous and barren quartz–quartz-molybdenite veins from the upthrown Continental block. In this area, the three vein types are similar petrographically, and fluid inclusion populations and microthermometric behavior among the vein types are indistinguishable.

Brimhall (1977) estimated early dark micaceous vein formation temperatures between 550° and 700°C, based on K and Na partitioning between K-feldspar and muscovite in vein envelopes. Roberts (1973) estimated the temperature of early dark micaceous vein formation between 550° and 700°C, based on the composition of coexisting ilmenite and hematite in alteration envelopes. Field et al. (2005) estimated temperatures between 550° and 650°C for the formation of quartz-molybdenite veins, based on sulfur isotope geothermometry on adjacent molybdenite and anhydrite grains. Rusk et al. (2006) estimated temperatures of formation of these veins between 550° and 650°C, based on the titanium in quartz geothermometer of Wark and Watson (2006).

The vast majority of B35 inclusions in deep, early dark micaceous and barren quartz–quartz-molybdenite veins homogenize between 330° and 370°C. An isochoric adjustment of several hundred degrees is therefore necessary to determine pressure of trapping. In the temperature range of 550° to 650°C, isochores for a 4 wt percent NaCl fluid containing 5 mol percent CO_2 with a density between 0.63 and 0.68 g/cm^3 (corresponding to homogenization temperatures between 340° and 360°C) indicate pressures between 170 and 270 MPa, with the majority of inclusions indicating between 200 and 250 MPa (Fig. 15). The presence of a few deep, quartz-molybdenite veins with aplitic centers (aplitic vein dikes) supports the suggestion that some of these veins formed at near-magmatic pressures and temperatures.

Early dark micaceous and pale-green sericitic veins from moderate and shallow depths: As noted by Roberts (1975), fluid inclusions in early dark micaceous and pale-green sericitic veins from moderate and shallow depths west of the Continental fault are more abundant and more variable compared to other vein types at Butte. Many early dark micaceous veins west of the Continental fault are overprinted by later mineralization, which has modified vein and alteration minerals complicating fluid inclusion petrography. Anhydrite, andalusite, and plagioclase, which are present in early dark micaceous alteration east of the Continental fault, are not present in the alteration envelopes of early dark micaceous or pale-green sericitic veins from west of the Continental fault.

Temperatures of formation of early dark micaceous veins are inferred to have been ~550° to 650°C, based on the estimates noted above and on the close temporal relationship between early dark micaceous veins and porphyry dike intrusion (Reed, 1999). Approximate pressures of fluid unmixing can be estimated based on the salinity of B15H inclusions. In a pure H_2O-NaCl system, the solvus for a 4 wt percent NaCl fluid (such as is trapped in B35 inclusions) at 600°C lies at about 84 MPa (Bodnar et al., 1985), and decompression to ~80 MPa would generate a fluid with 38 wt percent NaCl equiv (avg salinity of B15H inclusions) (Fig. 16). However, the addition of 5 mol percent CO_2 to a 4 wt percent NaCl equiv fluid would increase the pressure of unmixing by about 10 MPa at this temperature (extrapolated from Gehrig et al., 1986). The range of salinities in B15H inclusions suggests that unmixing occurred over a range of pressures between about 80 and 94 MPa at 600°C in early dark micaceous veins. Precise conditions of unmixing cannot be determined, however, owing to postentrapment modification of many B15H inclusions and the lack of data for the position of the solvus in the H_2O-NaCl-CO_2 system.

Reed and Rusk (2001) and Reed et al. (2005) inferred that pale-green sericitic veins are the upward extensions of early dark micaceous veins, based on their deposit-scale distribution and the observed change from early dark micaceous to pale-green sericitic alteration along strike of individual veins. Thermodynamic modeling and these geologic observations suggest that pale-green sericitic veins formed at cooler temperatures and lower pressures than early dark micaceous veins, but from the same fluids (Reed, 1999). Based on thermodynamic modeling, homogenization of vapor-rich inclusions at temperatures of up to 520°C and well-constrained temperatures of early dark micaceous vein formation, most pale-green sericitic veins probably formed between 475° and 550°C (Fig. 15). Fluid inclusion populations in pale-green sericitic veins are similar to those in moderate and shallow

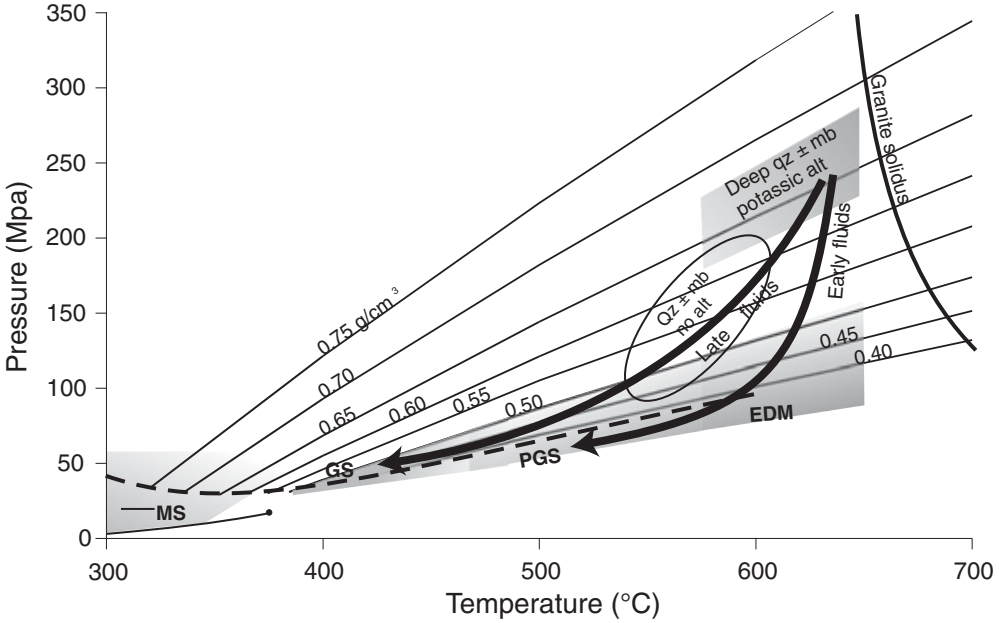

FIG. 15. Pressure-temperature diagram with isochores for a fluid containing 4 wt percent NaCl, and 5 mol percent CO_2 showing the inferred formation conditions of veins from Butte. Most deep, quartz-rich veins with early dark micaceous (EDM) or K-feldspar alteration formed between 200 and 250 MPa at temperatures between 575° and 650°C. Early dark micaceous veins formed where some depressurized fluids unmixed into vapor and brine and cooled in the range of 575° to 650°C and pressures of about 70 to 90 MPa. Pale-green sericitic (PGS) veins formed from continued cooling and reaction of these fluids in the range of 475° to 575°C and 50 to 80 MPa. Unmixing was less common in pyrite-quartz veins, produced from continued cooling of the magmatic fluid to temperatures near 400°C. Gray sericitic (GS) veins formed at pressures between 40 and 70 MPa. Main stage veins formed later from fluids between 230° and 400° degrees at pressures between 20 and 60 MPa. The dashed curve represents the limits of the miscibility gap in the system H_2O-CO_2-NaCl.

early dark micaceous veins; however, B15H and B85 inclusions are more abundant in pale-green sericitic veins. Similar to early dark micaceous veins, the abundance of B60, B15H, and B85 inclusions and the lack of B35 inclusions suggests that B35 fluids decompressed, forming B60 fluids which further decompressed and unmixed during ascent in fractures feeding pale-green sericitic veins. The absence of fluid inclusions with greater than 48 wt percent NaCl equiv in pale-green sericitic veins suggests that pressure dropped to no more than about 10 to 20 MPa below the estimated solvus of the fluid (Fig. 16). At 500°C, pressures of unmixing in pale-green sericitic veins are estimated to be between 50 and 70 MPa (Fig. 16); however, as with early dark micaceous veins, precise conditions cannot be determined. B60 inclusions in early dark micaceous and pale-green sericitic veins were trapped at slightly higher pressures, just above the solvus. The presence of inclusion clusters containing only B15H or only B85 inclusions in early dark micaceous and pale-green sericitic veins indicates that local physical separation of vapor and brine occurred.

Barren quartz/quartz-molybdenite veins from moderate depth: No independent estimations of temperature of formation of barren quartz–quartz-molybdenite veins from moderate depth are available because they contain only quartz and are accompanied by little or no alteration. We infer, based on sulfur isotope data from deeper quartz-molybdenite veins (Field et al., 2005), that these veins formed at temperatures similar to or slightly less than deeper, quartz-dominated veins.

Barren quartz–quartz-molybdenite veins from moderate depths are dominated by B35 and B60 inclusions; however, the distinction between B35 and B60 inclusions is not always clear. Many inclusions in these veins contain 40 to 60 vol percent vapor bubble, implying that their densities are between ideal B35 and ideal B60 inclusions, consistent with formation at slightly lower pressure than B35 inclusions in deeper barren quartz–quartz-molybdenite veins. The dominance of B35, B60, and inclusions with densities between B35 and B60 inclusions in quartz-molybdenite veins from moderate depths suggests that pressure fluctuated between 80 and 200 MPa at temperatures between 500° and 600°C, generating fluids ranging in density from about 0.40 to 0.65 g/cm^3. The presence of subordinate amounts of B15H, B85, and B20 inclusions record occasional unmixing at slightly lower pressures below the solvus (Fig 15).

Gray sericitic veins: Gray sericitic veins exist at shallow levels in the deposit, upward and outward from early dark micaceous and pale-green sericitic veins, and they dominate the central zone of pervasive sericitic alteration from the surface to depths greater than the deepest drilling. In shallow pyrite-quartz veins, euhedral quartz crystals contain few fluid inclusions. Vein quartz appears to have similar ratios of fluid inclusions as that of wall-rock quartz, but they are significantly fewer in quantity. Vein quartz and nearby igneous quartz are dominated by B60 and B85 inclusions. B15H inclusions are also present in some gray sericitic veins, and B20 inclusions are more abundant than in any other vein type. B35 inclusions are rare.

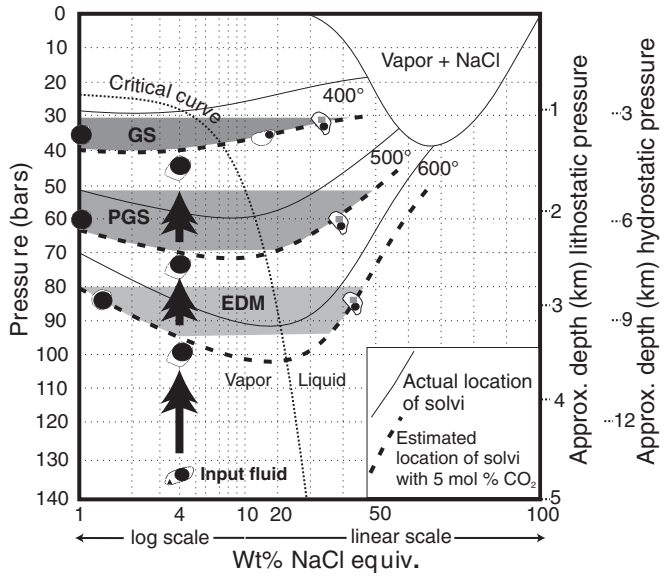

FIG. 16. Phase diagram showing the positions of the solvi in the system H_2O-NaCl (Sourirajan and Kennedy, 1962; Urusova, 1975; Bodnar et al., 1985). The positions of the solvi in the system CO_2-H_2O-NaCl have not been experimentally determined; however, we extrapolate the possible position of the solvi based on the work of Gehrig et al. (1986). The presence of 5 mol percent CO_2 increases the pressure of the solvus by about 15 MPa at 400° and ~10 MPa at 600°. The approximate pressures of unmixing of a 4 wt percent NaCl, 5 mol percent CO_2 fluid at 400°, 500°, and 600° are shown. The shaded regions correspond to approximate pressure-temperature conditions of unmixing in gray sericitic (GS), pale-green sericitic (PGS), and early dark micaceous (EDM) veins, respectively. The shapes of the solvi in the system CO_2-H_2O-NaCl have not been determined, so the positions and shapes are only estimates and precise pressures of unmixing cannot be made based on these solvi. Schematic diagrams of fluid inclusions show the fluid inclusion type generated at different pressures and temperatures.

Homogenization of B60 inclusions at minimum temperatures of ~370°C places lower limits on the temperature of gray sericitic vein formation. Thermodynamic modeling suggests that temperatures less than 450°C are necessary to form a fluid of sufficient acidity to generate sericitic alteration (Meyer and Hemley, 1967; Reed and Rusk, 2001; Reed et al., 2005). The low salinity, CO_2-bearing fluids trapped in B60 inclusions in and adjacent to gray sericitic veins were trapped between about 40 MPa at 370°C (estimated pressure of the solvus at 370°C) and about 70 MPa at 450°C (Fig. 15). These pressure and temperature conditions are slightly below, at, and above the approximate location of the critical point for trapped B60 fluids, which is ~390°C and 41 MPa, based on critical homogenization of B60 fluid inclusions. This estimate of the critical point of B60 fluids from Butte agrees with estimates of the critical point from Gehrig et al. (1986) and Schmidt and Bodnar (2000) for fluids of similar bulk composition. The presence of B15H, B85, and B20 inclusions in these veins suggests that pressures occasionally dropped slightly below the solvus and led to fluid unmixing. In gray sericitic veins, the wide variation of salinity in B20 inclusions results from the broadness of the solvus at low temperature and pressure (Fig. 16).

Main stage veins: The complexity of the Main stage hydrothermal system warrants a fluid inclusion study of its own; however, several samples were analyzed in this study for completeness. We examined about 20 Main stage veins and have analyzed 5. Only low salinity $B20_{MS}$ inclusions, some of which contain a small amount of dissolved CO_2, were identified. No halite-bearing or vapor-rich inclusions are present, indicating that boiling did not occur.

Assemblages of fluid inclusions in quartz from veins in the central Cu-rich, high-sulfur zone, and in quartz, rhodochrosite, and sphalerite from peripheral Pb-, Zn-, Mn-dominated veins contain low salinity fluid inclusions that homogenize between 230° and 340°C. There is no apparent difference in inclusion populations or microthermometric behavior between the two zones. We estimate a minimum pressure of 20 MPa based on lack of evidence for boiling, and a maximum of 60 MPa based on pressures estimated for gray sericitic veins, which are earlier and deeper than MS veins. Between 20 and 60 MPa, the range of trapping temperatures of $B20_{MS}$ fluids is from 230° to 400°C (Fig. 15).

Implications for Porphyry Cu Deposit Formation

Unusually great depth of the Butte hydrothermal system

The depth of formation of porphyry Cu-Mo deposits is typically difficult to determine and in many deposits it is poorly known (cf. Bodnar and Beane, 1980; Seedorff at al., 2005). In some cases depth can be reliably inferred from geologic relationships. Fluid inclusions may provide estimates of trapping pressure, but the resultant depth estimates are not straightforward because pressures may be either lithostatic or hydrostatic or somewhere in between. Most porphyry-type deposits apparently deposit ores at ~1 to 5 km depth, but the Butte deposit appears to be deeper.

At Butte, besides fluid inclusions, we have only indirect geologic estimates of depth. The Butte Quartz Monzonite is emplaced into folded and fault-thickened rocks of the Laramide fold and thrust belt (Tilling, 1973). The carapace of cogenetic late Cretaceous Elkhorn Mountains Volcanics is missing over the Butte Quartz Monzonite in the Butte district, supporting deep erosion. Applying the Al in Hornblende geobarometer (Anderson and Smith, 1995) to 10 samples of Butte Quartz Monzonite, Dilles et al. (1999) estimated that the Butte Quartz Monzonite crystallized at ~9.5 km depth near the Continental Pit and ~7.5 km depth near the Berkeley Pit, consistent with >1 km of normal displacement along the Continental fault. The error of calibration of this method is ±60 MPa or ± 2 km, but the Butte Quartz Monzonite hornblende is homogeneous, and sample variation yielded smaller errors of ±0.4 to ±0.7 km (1 std dev error based on 10–20 grains analyzed). The Butte Quartz Monzonite was, however, emplaced ~10 m.y. prior to porphyry Cu-Mo mineralization at Butte, so this estimate does not directly yield mineralization depths.

If B35 inclusions in deep, quartz-rich veins were trapped at temperatures of about 600°C, then pressures of vein formation were in the range of 200 to 250 MPa. Under lithostatic pressures, where rock density is 2.85 gm/cm^3, deep quartz veins within and beneath the zone of abundant molybdenite but below the zone of abundant chalcopyrite formed at depths of 6 to 9 km. This depth estimate coincides with that for the crystallization of the host Butte Quartz Monzonite; however, this is a greater depth than is inferred for any other porphyry Cu (Mo) deposit.

If this depth of formation is correct, then pressures inferred from fluid inclusion data suggest that most Cu mineralization occurred in early dark micaceous and pale-green sericitic veins at depths between 5 and 9 km. The depth of formation of deep barren quartz–quartz-molybdenite veins may be overestimated if temperature of vein formation is overestimated, if the densities of B35 fluids are overestimated, if the fluid cooled slightly before trapping, or if the magma-hydrothermal system was overpressured. Overpressurization may result from an interconnected fracture network reaching the magma below, which would translate pressure upward into the fluid in the sealed fracture network above (Carrigan et al., 1992).

Fluid inclusion petrography strongly supports the suggestion that Butte formed at greater depths than has been interpreted for other porphyry Cu deposits. That the Butte deposit formed at greater depth than the 1 to 5 km typical of most other porphyry Cu deposits is supported by several observations: (1) Butte deep veins lack B15H inclusions and are dominated instead by CO_2-rich B35 inclusions, veins containing only B35 inclusions have not been identified in any other deposit; (2) B15H inclusions are far less common at Butte than in most other deposits, which indicates that at Butte the pressure was commonly greater than that required to generate fluid unmixing; (3) B15H inclusions are less saline (average of 38 wt % NaCl equiv) than is typical in many other porphyry Cu deposits (35–70 wt % NaCl equiv) and these salinities indicate pressures only slightly less than the solvus generating immiscibility; (4) B60 inclusions, present in all vein types below, within, and above the main Cu-ore zone imply pressures intermittently in the one-phase field, above the fluid solvus during vein formation throughout the evolution of the hydrothermal system.

Butte may be rare among porphyry Cu deposits for its great depth of formation. Sufficient uplift, erosion, and exploration have taken place to reveal abundant, CO_2-bearing, low salinity fluid inclusions that are samples of a single-phase parental magma-derived aqueous fluid. In many porphyry Cu deposits the exposure is not deep enough to reveal the deepest parts of the system where a single-phase hydrothermal fluid is predicted. Similar low salinity fluids have been recognized and described in deep veins from the Alta Stock, Utah (John, 1989); Bingham Canyon, Utah (Redmond et al., 2004); and Questa, New Mexico (Cline and Bodnar, 1994). Rusk et al. (2007) also identified similar inclusions, typically in the presence of multiple inclusion populations, in deep veins from numerous porphyry deposits (Henderson and Climax, Colorado; Copper Creek and Mineral Park, Arizona; and El Salvador, El Teniente, Los Pelambres, and Chuquicamata, Chile). These occurrences suggest that parental low salinity inclusions are more common than previously recognized and future studies of deeper parts of porphyry ore systems will likely reveal similar fluid inclusions.

Evolution of a single parental hydrothermal fluid formed the Butte deposit

To account for the variation in vein and alteration types in some porphyry Cu deposits, previous studies suggested a magmatic origin of fluids that form early potassic alteration and a meteoric fluid origin for later sericitic alteration based on oxygen and hydrogen isotope studies (Sheppard and Taylor, 1974; Sheppard and Gustafson, 1976; Taylor, 1997). This interpretation was reinforced by the presence of low salinity aqueous inclusions, common in sericitically altered pyrite-quartz veins from porphyry Cu deposits, which were interpreted to have trapped dilute meteoric fluids during late quartz-sericite-pyrite mineralization (Gustafson and Hunt, 1975; Nash, 1976; Eastoe, 1978; Preece and Beane, 1982; Reynolds and Beane, 1985; Beane and Bodnar, 1995). More recently, however, magmatic fluids have been implicated in the formation of pyritic veins with sericitic alteration at Far Southeast (Hedenquist et al., 1998), Butte (Zhang, 2000; Rusk et al., 2004), Alumbrera (Harris et al., 2005), Refugio district (Muntean and Einaudi, 2001), the Endeavor 26 North deposit (Harris and Golding, 2002), and Henderson (Seedorff and Enauidi, 2004). Whereas Hedenquist et al. (1998) and Muntean and Einaudi (2001) call upon influx of multiple magmatic fluids of varying composition to form early potassic and later sericitic alteration, Seedorff and Einaudi (2004) conclude that the transition from potassic to sericitic alteration at the Henderson porphyry Mo deposit was promoted by a change in temperature rather than a change in fluid composition. At Butte, we infer that the entire suite of vein and alteration types was produced by various reaction paths of a single parental magma-derived hydrothermal fluid. This parental fluid apparently maintained relatively constant initial composition throughout the life of the hydrothermal system.

The bulk chemical compositions of low salinity inclusions in early potassically altered veins and late pyrite veins with sericitic alteration are similar and indicate little compositional change of the hydrothermal fluid extracted from the magma over the life of the magmatic-hydrothermal system. We therefore conclude that variations in ore mineral and alteration mineral assemblages derive from chemical changes in the fluid resulting from the various cooling and depressurization paths of the parental B35 fluid and the reaction history of the rock through which the fluid flowed rather than from pulses of magmatic fluids of varying initial compositions. For example, we infer that quartz-rich veins (±molybdenite) with little alteration form from fluid depressurization at high temperatures where the solubility of quartz is very high (Fournier, 1999, Rusk and Reed, 2002). When this fluid cooled under transiently hydrostatic conditions, occasional unmixing occurred and chalcopyrite-rich, magnetite-bearing, early dark micaceous and subsequent pale-green sericitic veins formed. Later, as the same parental fluid cooled further at lower pressures, it became progressively more acidic and formed pyrite-dominated veins with abundant sericitc alteration (Fig. 15). This interpretation agrees with thermodynamic modeling, which shows that the entire range of alteration types at Butte can be derived from the interaction of the Butte Quartz Monzonite with a cooling fluid similar in composition to B35 inclusions (Reed et al., 2005).

Nearly constant salinity and CO_2 concentration in early and late veins is not consistent with models of "closed system" magma crystallization, which predict that as crystallization progresses both the Cl/H_2O and the CO_2/H_2O ratios should change (Candela and Holland, 1986, Cline and Bodnar, 1991). Therefore, the compositional similarity implies either degassing of only a small percent of a large volume of magma or input of volatiles from external sources at depth.

It is likely that a significant volume of magma crystallized during the several-million-year span of the Butte hydrothermal system (Martin et al., 1999; Snee et al., 1999; Dilles et al. 2004). Evidence of progressively cooler mineralizing events in a given space indicates the loss of heat in the hydrothermal system and cooling and crystallization of the underlying magma. Our results imply that rather than being the product of a single magma crystallizing in a closed system, the hydrothermal system at Butte was repeatedly or continuously recharged by external magmatic volatile sources and/or by convection within a large magma chamber. Underplating of silicic magma chambers by mafic magmas is common in the roots of arc batholiths (DeBari and Coleman, 1989; Wiebe, 1996) and is also recognized in active volcanic systems such as Pinatubo (de Hoog et al., 2004). Comingling of mafic and silicic magmas in porphyry intrusions and volcanic rocks related to porphyry Cu deposits has been recognized by Halter et al. (2004) and Hattori and Keith (2001). Nearly constant parental fluid compositions throughout the span of pre-Main stage mineralization imply that the source of magmatic volatiles at Butte behaved as an open system and was recharged with volatiles derived from external sources.

Time and space evolution of hydrothermal fluids

An interpretation of the evolution of the hydrothermal system is illustrated in Figure 17, which shows the time and space relationships observed among vein and fluid inclusion types. During the evolution of the hydrothermal system, a magma at depth continuously supplied low salinity, CO_2-bearing, Cu-rich aqueous fluids. These fluids evolved by local vapor-brine immiscibility and by compositional change resulting from pressure and temperature variations, wall-rock reaction, and vein precipitation to form quartz-dominated (± molybdenite) veins, chalcopyrite and magnetite-bearing early dark micaceous and pale-green sericitic veins, as well as postore gray sericitic veins. Deep in the hydrothermal system, under lithostatic pressure, at depths of 6 to 9 km and temperatures near 600°C, low salinity fluids precipitated quartz-rich, molybdenite-bearing veins with little chalcopyrite and with minor potassic alteration envelopes. These veins formed largely in response to fluid depressurization. Upon dike intrusion and thereafter, this fluid ascended and cooled under transiently hydrostatic conditions to form early dark micaceous veins at moderate depths, pressures between 60 and 90 MPa, and temperatures of about 600°C. At slightly shallower depths, pale-green sericitic veins formed as this same fluid continued to ascend, cooled to about 475°C at pressures between 50 and 70 MPa, frequently unmixed, and continued to react with wall rock. Later in the evolution of the deposit, as the hydrothermal system cooled, low salinity magmatic fluids depressurized and cooled at temperatures and pressures usually above the brine-vapor solvus, forming barren quartz–quartz-molybdenite veins with no alteration at moderate depths and gray sericitic veins and alteration at shallower depths as the fluid cooled to about 370°C (Fig. 15). As the hydrothermal system waned and continued to cool, gray sericitic veins advanced downward, overprinting much of the previous mineralization. Main stage veins formed at shallower depths than gray sericitic veins, where magma-derived acidic aqueous fluids rich in metals cooled, decompressed, and mixed with meteoric waters at hydrostatic pressures (Garlick and Epstein, 1967; Sheppard and Taylor, 1974; Brimhall, 1979; Zhang, 2000; Rusk et al., 2004; Field et al., 2005).

Origin and precipitation of chalcopyrite and molybdenite

Recent fluid inclusion microthermometry and LA-ICP-MS studies have suggested that cooling of Cu-rich brines to temperatures below 400°C is responsible for chalcopyrite precipitation at Bingham Canyon (Landtwing et al., 2005) and Alumbrera (Ulrich et al., 2001). On the other hand, Dilles and Einaudi (1992) concluded that at Yerington, chalcopyrite precipitation took place at high temperatures during potassic alteration. Their arguments are based on the observation that chalcopyrite-bearing veins with potassic alteration are cut by porphyry dikes, which were then later cut by pyrite veins with sericitic veins at temperatures near 400°C, indicating that fluid cooling to temperatures below 400°C occurred after chalcopyrite precipitation.

At Butte, chalcopyrite is most abundant in and around pale-green sericitic and early dark micaceous veins which we infer to have formed from a fluid cooling from ~650° to ~475°C. Cooling of the hydrothermal system to temperatures in the range of 400°C led to sericitic alteration, which contains subeconomic Cu grades and clearly postdates early dark micaceous and pale-green sericitic vein formation. It is highly unlikely that a late fluid, at temperatures less than 400°, could selectively infiltrate early dark micaceous and pale-green sericitic veins and precipitate chalcopyrite, leaving no wall-rock alteration to suggest its presence. We therefore conclude that chalcopyrite precipitation at Butte occurred at the elevated temperatures and pressures implied for the formation of early dark micaceous and pale-green sericitic veins.

Both brine and vapor-rich inclusions are ubiquitous in porphyry Cu deposits, and the presence of chalcopyrite daughter minerals in either inclusion type in various deposits implicates both fluid phases as efficient Cu-transporting mediums (Ulrich et al., 2001; Bouzari and Clark, 2006). B35 inclusions, many with chalcopyrite daughter minerals, contain up to 1 wt percent Cu (avg ~4,000 ppm Cu: Rusk et al., 2004) and are the dominant inclusion type in the Continental block (Cu grades from ~0.2 to 0.4%), which indicates that these fluids were also efficient transporters of Cu. Textures such as those in Figure 5H, where primary (?) chalcopyrite-bearing fluid inclusions are trapped in euhedral quartz crystals containing small chalcopyrite crystals and projecting into chalcopyrite, also suggest that B35 fluids precipitated chalcopyrite at depth. Low salinity B35 fluids with high Cu concentrations imply that high salinity fluids are not necessary to form a large porphyry deposit (cf. Candela and Holland, 1986) and are consistent with experiments of Simon et al. (2006) that show that sulfur species are likely important ligands transporting Cu in the hydrothermal fluid.

Whereas it is apparent that some chalcopyrite precipitated directly from the single-phase fluid in deep, quartz-rich veins, higher Cu grades (0.6-0.9 wt % Cu) are at shallower levels in the deposit, coincident with the zone of abundant early dark micaceous and pale-green sericitic veins (magnetite zone: Fig. 2). These veins contain more vapor and brine inclusions than any other vein type. Hence, fluid inclusion relationships indicate that unmixing of B35 fluids to form B15H and B85

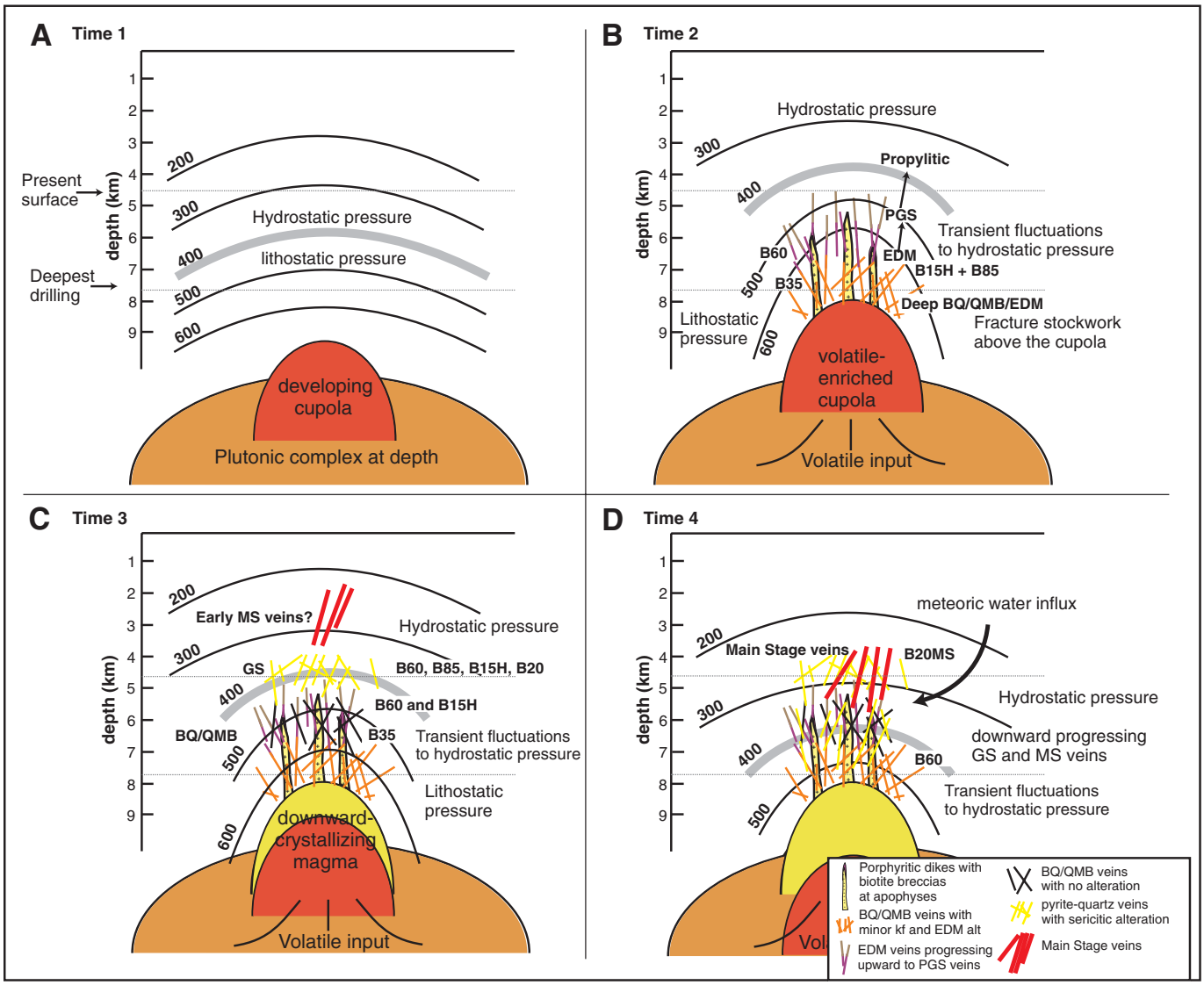

FIG. 17. Schematic diagram depicting the evolution of the hydrothermal system at Butte. A) In this model, a large pluton at depth develops a volatile-charged cupola at its top. B) Quartz-porphyry dikes intrude the Butte Quartz Monzonite, initiating the hydrothermal system. At depth, where the country rock is hottest, little cooling of fluid occurs and lithostatic pressure dominates. B35 fluid inclusions are trapped in quartz-rich veins under these conditions. As single-phase fluids (B35) ascend, they unmix to B15H and B85 fluids as a result of transient fluctuations in hydrostatic pressure. Rates of fluid cooling are slow relative to depressurization due to the depth and high temperature of the hydrothermal system. Early dark micaceous (EDM), pale-green sericitic (PGS), and propylitic veins and alteration form as fluids at magmatic temperatures progressively ascend, cool, and react with Butte Quartz Monzonite (BQM). C) Barren quartz (BQ) and quartz-molybdenite (QMB) veins prograde upward forming from fluids cooling and depressurizing mostly above the fluid solvus. At shallower depths, above most early dark micaceous, pale-green sericitic, and barren quartz–quartz-molybdenite veins, gray sericitic (GS) veins form where fluids cool to ~400°C, which causes the fluid to become highly acidic, leading to sericitic alteration. Rates of fluid cooling relative to depressurization were greater than in earlier, deeper mineralization. D) As the magmatic system continues to crystallize and cool, isotherms retreat downward. Gray sericitic veins form at progressively greater depths, cutting all earlier vein types. Main stage veins form at shallow levels where magmatic and meteoric fluids mix.

fluids enhanced chalcopyrite (and magnetite) precipitation. In addition to brine-vapor immiscibility, fluid cooling and fluid-rock reactions are implicated in chalcopyrite precipitation by wide early dark micaceous and pale-green sericitic alteration envelopes containing chalcopyrite in mafic sites.

We infer that B35 fluids were also the source of Mo mineralization, based on the dominance of these inclusions in quartz-molybdenite veins that contain the preponderance of Mo at Butte. The dominance of B35 inclusions and the lack of evidence for fluid unmixing in many quartz-molybdenite veins suggest that Mo was both transported by and precipitated from these fluids. Cathodoluminescence images suggest that quartz and molybdenite precipitated simultaneously, with no evidence for the introduction of molybdenite by later hydrothermal fluids (Rusk, 2003). Fluid inclusions, the presence of molybdenite only in veins with >90 percent quartz, and lack

of alteration around these veins suggest that molybdenite and quartz precipitated upon pressure drop from near-lithostatic to near-hydrostatic conditions (Rusk and Reed, 2002).

Precipitation of Cu by a different mechanism than Mo at Butte is consistent with experimental and thermodynamic considerations of Cu and Mo solubility. Both Cl and S complexes have been implicated in Cu transport in aqueous fluids (Candela and Holland, 1984; Simon et al., 2006), whereas Candela and Holland (1984) and Zotov et al. (1995) suggest instead that Mo is transported as MoO_2 or $HMoO_4^-$. Liu and McPhail (2005) and Hemley et al. (1992) show that Cu solubility increases slightly in hydrothermal fluids with decreasing pressure. Temperature decrease is therefore far more likely than pressure decrease to drive Cu precipitation, as we infer at Butte. The effects of pressure and temperature on molybdenite solubility at the pressure and temperature range of interest are not well known.

Conclusions

Our results, along with those of Roberts (1975), suggest that Butte is one of the deepest porphyry Cu deposits known. The great depth of formation of the Butte deposit is recorded by the predominance of fluids trapped above the solvus in the H_2O-NaCl-CO_2 system in deep, quartz-dominated veins. Fluid inclusion distribution, compositions, and homogenization behavior combined with LA-ICP-MS data on metal contents (Rusk et al., 2004) document that B35 fluids are samples of magma-derived aqueous fluids characterized by low salinity, moderate CO_2 contents, and up to 1 wt percent Cu. Such parental fluids scavenged Cu and Mo from the melt below and transported them to the hydrothermal system above. Given that a low salinity fluid provided the bulk of Cu, Mo, and S at Butte, we conclude that NaCl-rich brines are not essential for the extraction or transport of Cu or Mo from a crystallizing melt to generate a large porphyry Cu-Mo deposit. The increased abundance of B15H and B85 inclusions coinciding with the highest grade pre-Main stage (porphyry Cu) mineralization at Butte suggests that brine-vapor unmixing plays an important role in Cu-ore precipitation and deposit-wide metal and alteration zonation. In addition to unmixing, cooling and water-rock reaction also played an important role in chalcopyrite precipitation at Butte. Fluid inclusion evidence and vein-cutting relationships indicate that chalcopyrite mineralization occurred at high temperatures coinciding with potassic alteration, rather than from later, lower temperature fluids. Fluid immiscibility does not appear to have been an important factor in the precipitation of molybdenite, which is most abundant in the region dominated by B35 inclusions. Compositions, deposit-scale distribution, and trapping conditions of fluid inclusions can be explained by the continued influx of a parental low salinity magmatic hydrothermal fluid, with no significant change in the bulk composition of the input fluid over the integrated lifetime of ore metal precipitation and vein formation. Variations in the temperature-pressure–wall-rock reaction path account for the sequence of vein formation from early quartz-dominated veins with potassic alteration to late pyrite-dominated veins with sericitic alteration. Early fluids decompressed rapidly relative to cooling, forming quartz-rich veins with potassic alteration at depth and chalcopyrite-magnetite-bearing early dark micaceous and pale-green sericitic veins at shallower levels in the deposit. Later, as the hydrothermal system waned, the rate of decompression relative to fluid cooling slowed, causing the fluid to remain above its solvus, forming pyrite veins with sericitic alteration which overprint much of the deposit.

Acknowledgments

This research was funded by National Science Foundation grants EAR 0001272 and EAR 0440198. The U.S. Geological Society Mendenhall postdoctoral fellowship program also provided material support. We thank Steve Czehura, Dick Berg, George Burns, Cyrus Field, Lihua Zhang, Bob Houston, Sebastian Geiger, and Jim Reynolds for discussions, assistance, and comments which aided in the completion of this study. The original manuscript was improved by thoughtful and insightful reviews from Adam Simon and Bob Bodnar.

June 26, December 10, 2007

REFERENCES

Anderson, J.L., and Smith, D.R., 1995, The effects of temperature and f_{O_2} on the Al-in-hornblende barometer: American Mineralogist, v. 80, p. 549–559.

Arribas, A, Jr., Hedenquist, J.W., Itaya, T., Okada, T., Concepcion, R.A., and Garcia, J.S., Jr., 1995, Contemporaneous formation of adjacent porphyry and epithermal Cu-Au deposits over 300 ka in Northern Luzon, Philippines: Geology, v. 23, p. 337–340.

Audétat, A., and Günther, D., 1999, Mobility and H_2O loss from fluid inclusions in natural quartz crystals: Contributions to Mineralogy and Petrology, v. 137, p. 1–14.

Audétat, A., Günther, D., and Heinrich, C.A., 2000, Magmatic-hydrothermal evolution in a fractionating granite: A microchemical study of the Sn-W-F-mineralized Mole Granite, Australia: Geochimica et Cosmochimica Acta, v. 64, p. 3373–3393.

Azbej, T., Severs, M.J., Rusk, B.G., and Bodnar, R.J., 2007, In situ quantitative analysis of individual H_2O-CO_2 fluid inclusions by laser Raman spectroscopy: Chemical Geology, v. 237, p. 255–263.

Bakker, R.J., 1997, Clathrates: Computer programs to calculate fluid inclusion V-X properties using clathrate melting temperatures: Computers and Geosciences, v. 23, p. 1–18.

Bakker, R.J., Dubessy, J., and Cathelineau, M., 1996, Improvements in modelling: I. The H_2O-CO_2 system with various salts: Geochimica et Cosmochimica Acta, v. 60, p. 1657–1681.

Beane, R.E., and Bodnar, R.J., 1995, Hydrothermal fluids and hydrothermal alteration in porphyry copper deposits, *in* Pierce, F.W., and Bohm, J.G. eds., Porphyry copper deposits of the American Cordillera: Tucson, AZ, Arizona Geological Society Digest 20, p. 83–93.

Beane, R.E., and Titley, S.R., 1981, Porphyry copper deposits. Part II. Hydrothermal alteration and mineralization: Economic Geology 75th Anniversary Volume, p. 235–269.

Becker, S.P., Fall, A., and Bodnar, R.J., 2008, PVTX properties of high salinity H_2O-NaCl Solutions (>30 wt % NaCl equiv): Application to fluid inclusions that homogenize by halite disappearance from porphyry copper and other hydrothermal ore deposits: Economic Geology, in press.

Bischoff, J.L., and Pitzer, K.S., 1985, Phase relations and adiabats in boiling seafloor geothermal systems: Earth and Planetary Science Letters, v. 75, p. 327–338.

Bodnar, R.J., 1993, Revised equation and table for determining the freezing point depression of H_2O-NaCl solutions: Geochimica et Cosmochimica Acta, v. 57, p. 683–684.

——1994, Synthetic fluid inclusions: XII. The system H_2O-NaCl. Experimental determination of the halite liquidus and isochores for a 40 weight percent NaCl solution: Geochimica et Cosmochimica Acta, v. 58, p. 1053–1063.

——1995, Fluid inclusion evidence for a magmatic source for metals in porphyry copper deposits, *in* Thompson, J. ed., Magmas, fluids, and ore deposits: Mineralogical Association of Canada Short Course, v. 23, p. 139–152.

Bodnar, R.J., and Beane, R.E., 1980, Temporal and spatial variations in hydrothermal fluid characteristics during vein filling in preore cover overlying deeply buried porphyry copper-type mineralization at Red Mountain, AZ: Economic Geology, v. 75, p. 876–893.

Bodnar, R.J., and Vityk, M.O., 1994, Interpretation of microthemometric data for H_2O-NaCl fluid inclusions, *in* DeVivo, B., and Frezzotti, M.L., eds., Fluid inclusions in minerals: Methods and Applications: Blacksburg, VA, Virginia Polytechnic Institute and State University, p. 117–130.

Bodnar, R.J., Burnham, C.W., and Sterner, S.M., 1985, Synthetic fluid inclusions in natural quartz. III. Determination of phase equilibrium properties in the system H_2O-NaCl to 1000°C and 1500 bars: Geochimica et Cosmochimica Acta, v. 49, p. 1861–1873.

Bouzari, F., and Clark, A.H., 2006, Prograde evolution and geothermal affinities of a major porphyry copper deposit: The Cerro Colorado hypogene protore, I Region, northern Chile: Economic Geology, v. 101, p. 95–134.

Bowers, T.S., and Helgeson, H.C., 1983, Calculation of the thermodynamic and geochemical consequences of nonideal mixing in the system H_2O-CO_2-NaCl on the relations in geologic systems: Equation of state for the H_2O-CO_2-NaCl fluids at high pressures and temperatures: Geochimica et Cosmochimica Acta, v. 47, p. 1247–1275.

Bowman, J.R., Parry, W.T., Kropp, W.P., and Kruer, S.A., 1987, Chemical and isotopic evolution of hydrothermal solutions at Bingham, Utah: Economic Geology, v. 82, p. 395–428.

Bozzo, A.T., Chen, H., Kass, J.R., and Barduhn, A.J., 1975, The properties of hydrates of chlorine and carbon dioxide: Desalination, v. 16, p. 303–320.

Brathwaite, R.L., Simpson, M.P., Faure, K., and Skinner, D.N.B., 2001, Telescoped porphyry Cu-Mo-Au mineralization, advanced argillic alteration and quartz-sulphide-gold-anhydrite veins in the Thames district, New Zealand: Mineralium Deposita, v. 36, p. 623–640.

Brimhall, G.H., Jr., 1977, Early fracture-controlled disseminated mineralization at Butte, Montana: Economic Geology, v. 72, p. 37–59.

——1979, Lithologic determination of mass transfer mechanisms of multiple-stage porphyry copper mineralization at Butte, Montana: Vein formation by hypogene leaching and enrichment of potassium silicate protore: Economic Geology, v. 74, p. 556–589.

Brown, R.G., 1894, The ore deposits of Butte City: Transactions of the American Institute of Mining and Metallurgical Engineering, v. 24, p. 543–558.

Brown, P., 1989, FlinCor: A microcomputer program for the reduction and investigation of fluid inclusion data: American Mineralogist, v. 74, p. 1390–1411.

Burnham, C.W., 1979, Magmas and hydrothermal fluids, *in* Barnes, H.L., ed., Geochemistry of Hydrothermal ore deposits, 2nd ed.: New York, John Wiley, p. 71–136.

Candela, P.A., and Holland, H.D., 1984, The partitioning of copper and molybdenum between silicate melts and aqueous fluids: Geochimica et Cosmochimica Acta, v. 48, p. 373–380.

——1986, A mass transfer model for copper and molybdenum in magmatic hydrothermal systems: The origin of porphyry-type ore deposits: Economic Geology, v. 81, p. 1–19.

Carrigan, C.R., Schubert, G., and Eichelberger, J., 1992, Thermal and dynamical regimes of single-and two-phase magmatic flow in dikes: Journal of Geophysical Research, v. 97, p. 377–392.

Carten, R.B., Geraghty, E.P., Walker, B.M., and Shannon, J.R., 1988, Cyclic development of igneous features and their relationship to high temperature hydrothermal features in the Henderson porphyry molybdenum deposit, Colorado: Economic Geology, v. 83, p. 266–296.

Chen, H., 1972, The thermodynamics and composition of carbon dioxide hydrate: Unpublished M.S. thesis, New York, Syracuse University, 67 p.

Cline, J.S., and Bodnar, R.J., 1991, Can economic porphyry copper mineralization be generated by a typical calc-alkaline melt?: Journal of Geophysical Research, v. 96, p. 8113–8126.

——1994, Direct evolution of brine from crystallizing silicic melt at the Questa, New Mexico, Molybdenum deposit: Economic Geology, v. 89, p. 1780–1802.

Collins, P.F., 1979, Gas hydrates in CO_2-bearing fluid inclusions and use of the freezing point data for estimation of salinity: Economic Geology, v. 74, p. 1435–1444.

Corn, R.M., 1975, Alteration-mineralization zoning, Red Mountain, AZ: Economic Geology, v. 70, p. 1437–1447.

DeBari, S.M., and Coleman, R.G., 1989, Examination of the deep levels of an island arc, the Tonsina ultramafic-mafic assemblage, Tonsina, Alaska: Journal of Geophysical Research, v. 94, p. 4373–4391.

de Hoog, J.C., Hattori, K.H., and Hoblitt, R.P., 2004, Oxidized sulphur-rich mafic magma at Mount Pinatubo, Philippines: Contributions to Mineralogy and Petrology, v. 146, p. 750–761.

Diamond, L.W., 1992, Stability of CO_2 clathrate hydrate + CO_2 liquid + CO_2 vapour + aqueous KCl-NaCl solutions: Experimental determination and application to salinity estimates of fluid inclusions: Geochimica et Cosmochimica Acta, v. 56, p. 273–280.

——1994, Salinity of multivolatile fluid inclusions determined from clathrate hydrate stability: Geochimica et Cosmochimica Acta, v. 58, p. 19–41.

Dilles, J.H., 1987, The petrology of the Yerington batholith, Nevada: Evidence for the evolution of porphyry copper ore fluids: Economic Geology, v. 82, p. 1750–1789.

Dilles, J.H., and Einaudi, M.T., 1992, Wall-rock alteration and hydrothermal flow paths about the Ann Mason porphyry copper deposit, Nevada, A 6-km vertical reconstruction: Economic Geology, v. 87, p. 1963–2001.

Dilles, J.H., Reed, M.H., Roberts, S., Zhang, L., and Houston, R., 1999, Early magmatic hydrothermal features related to porphyry copper mineralization at Butte, Montana [abs.]: Geological Society of America Abstracts with Programs, v. 31, no. 7, p. A380.

Dilles, J.H., Stein, H.J., Martin, M.W., and Rusk, B.G., 2004, Re-Os and U-Pb Ages for the Butte copper district, Montana [abs.]: IAVCEI Meeting, Púcon, Chile, <http://iavcei2004.free.cl/abstract_aprobation.asp>.

Duan, Z., Moller, N., and Weare, J.H., 1992a, and equation of state for the CH_4-CO_2-H_2O system: I. Pure systems from 0 to 1000°C and 0 to 8000 bars: Geochimica et Cosmochimica Acta, v. 56, p. 2605–2617.

——1992b, and equation of state for the CH_4-CO_2-H_2O system: II. Mixtures from 50 to 1000°C and 0 to 1000 bars: Geochimica et Cosmochimica Acta, v. 56, p. 2619–2631.

——1995, Equation of state for the NaCl-H_2O-CO_2 system; prediction of phase equilibria and volumetric properties: Geochimica et Cosmochimica Acta, v. 59, p. 2869–2882.

Dubessy, J., Thiery, R., and Canals, M., 1992, Modelling of phase equilibria involving mixed gas clathrates: application to the determination of molar volume of the vapour phase and salinity of the aqueous solution in fluid inclusions: European Journal of Mineralogy, v. 4, p. 873–884.

Eastoe, C.J., 1978, A fluid inclusion study of the Panhuna porphyry copper deposit, Bouganville, Papua New Guinea: Economic Geology, v. 73, p. 721–748.

Emmons, S.F., and Tower, G.W., Jr., 1897, Economic geology of the Butte special district [Montana]: U.S. Geological Survey, Atlas, Butte Folio no. 38, p. 3–8.

Field, C.W., Zhang, L., Dilles, J.H., Rye, R.O., and Reed, M.H., 2005, Sulfur and oxygen isotopic record in sulfate and sulfide minerals of early, deep, pre-Main stage porphyry Cu-Mo and late, shallow Main stage base-metal mineral deposits, Butte district, Montana: Chemical Geology, v. 215, p. 61–93.

Fournier, R.O., 1999, Hydrothermal processes related to movement of fluid from plastic into brittle rock in the magmatic-epithermal environment: Economic Geology, v. 94, p. 1193–1211.

Garlick, G.D., and Epstein, S., 1967, Oxygen isotope ratios in coexisting minerals of regionally metamorphosed rocks: Geochimica et Cosmochimica Acta, v. 31, p. 181–214.

Gehrig, M., Lentz, H., and Franck, E., 1986, The system water-carbon dioxide-sodium chloride to 773 K and 300 MPa: Physical Chemistry, v. 90, p. 525–533.

Geiger, S., Haggerty, R., Dilles, J., Reed, M., and Matthai, S, 2002, New insights from reactive transport modeling; the formation of sericitic vein envelopes during early hydrothermal alteration at Butte, Montana: Geofluids, v. 2, p. 185–201.

Goldfarb, R.J., Ayuso, R.A., Miller, M.L., Ebert, S., Marsh, E.E., and Petsel, S.A., 2004, The late Cretaceous Donlin Creek gold deposit, southwestern Alaska; controls on epizonal ore formation: Economic Geology, v. 99, p. 643–671.

Goldstein, R.H., and Reynolds, T.J., 1994, Systematics of fluid inclusions in diagenetic materials: Society for Sedimentary Geology Short Course 31, 199 p.

Gustafson, L.B., and Hunt, J.P., 1975, The porphyry copper deposit at El Salvador, Chile: Economic Geology, v. 70, p. 857–912.

Halter, W.E., Heinrich, C.A., and Pettke, T., 2004, Laser-ablation ICP-MS analysis of silicate and sulfide melt inclusions in an andesitic complex. II. Evidence for magma mixing and magma chamber evolution: Contributions to Mineralogy and Petrology, v. 147, p. 397–412.

Harris, A.C., and Golding, S.D., 2002, New evidence of magmatic-fluid related phyllic alteration: Implications for the genesis of porphyry copper deposits: Geology, v. 30, p. 335–338.

Harris, A.C., Golding, S.D., and White, N.C, 2005, Bajo de la Alumbrera copper-gold deposit: Stable isotope evidence for a porphyry-related hydrothermal system dominated by magmatic aqueous fluids: Economic Geology, v. 100, p. 63–86.

Hattori, K.H., and Keith, J.D., 2001, Contribution of mafic melt to porphyry copper mineralization: evidence from Mount Pinatubo, Philippines, and Bingham Canyon, Utah, USA: Mineralium Deposita, v. 36, p. 799–806.

Hedenquist, J., and Henley, R., 1985, The importance of CO_2 on freezing point measurements of fluid inclusions: Evidence from active geothermal systems and implications for epithermal ore deposition: Economic Geology, v. 80, p. 1379–1406.

Hedenquist, J., Arribas, A., and Reynolds, J., 1998, Evolution of an intrusion-centered hydrothermal system: Far Southeast-Lepanto porphyry and epithermal Cu-Au deposits, Philippines: Economic Geology, v. 93, p. 373–404.

Heinrich, C.A., Günther, D., Audétat, A., Ulrich, T., and Frischknecht, R., 1999, Metal fractionation between magmatic brine and vapor, determined by micro-analysis of fluid inclusions: Geology, v. 27, p. 755–758.

Hemley, J.J., Cygan, G.L., Fein, J.B., Robinson, G.R., and d'Angelo, W.M., 1992, Hydrothermal ore-forming processes in the light of studies in rock-buffered systems: I. Iron-copper-zinc-lead sulfide solubility relations: Economic Geology, v. 87, p. 1–22.

Houston, R.A., 2002, Geology and structural history of the Butte district, Montana: Unpublished M.S. thesis, Corvallis, Oregon, Oregon State University, 45 p.

John, D., 1989, Geologic setting, depths of emplacement, and regional distribution of fluid inclusions in intrusions of the central Wasatch Mountains, Utah: Economic Geology, v. 84, p. 386–409.

Khashgerel, B., Rye, R.O., Hedenquist, J.W., and Imants, K., 2006, Geology and Reconnaissance stable isotope study of the Oyu Tolgoi porphyry Cu-Au system, South Gobi, Mongolia: Economic Geology, v. 101, p. 503–522.

Landtwing, M.R., Pettke, T., Halter, W.E., Heinrich, C.A., Redmond, P.B., Einaudi, M.T., and Kunze, K., 2005, Copper deposition during quartz dissolution by cooling magmatic-hydrothermal fluids: The Bingham porphyry: Earth and Planetary Science Letters, v. 235, 229–243.

Larson, S.D., 1955, Phase studies of the two-component carbon dioxide-water system involving the carbon dioxide hydrate: Unpublished Ph.D. dissertation, Ann Arbor, University of Michigan, 301 p.

Liu, W., and McPhail, D.C., 2005, Thermodynamic properties of copper chloride complexes and copper transport in magmatic-hydrothermal solutions: Chemical Geology, v. 221, p. 21–39.

Lowell, J.D., and Guilbert, J.M., 1970, Lateral and vertical alteration-mineralization zoning in porphyry ore deposits: Economic Geology, v. 65, p. 373–408.

Lund, K., Aleinkoff, J., Kunk, M., Unruh, D., Zeihen, G., Hodges, W., Du Bray, E., and O'Neill, J., 2002, Shrimp U-Pb and $^{40}Ar/^{39}Ar$ age constraints for relating plutonism and mineralization in the Boulder batholith region, Montana: Economic Geology, v. 97, p. 241–267.

Manske, S.L., and Paul, A.H., 2002, Geology of a major new porphyry copper center in the Superior (Pioneer) district, Arizona: Economic Geology, v. 97, p. 197–220.

Martin, M.W., Dilles, J.H., and Proffett, J.M., 1999, U-Pb geochronilogic constraints for the Butte porphyry system [abs.]: Geological Society of America Abstracts with Programs, v. 31, no. 7, p. A380.

Mavrogenes, J.A., and Bodnar, R.J., 1994, Hydrogen movement into and out of fluid inclusions in quartz: Experimental evidence and geologic implications: Geochimica et Cosmochimica Acta, v. 58, p. 141–148.

Meyer, C., 1965, An early potassic type of wall rock alteration at Butte, Montana: American Mineralogist, v. 50, p. 1717–1722.

Meyer, C., and Hemley, J.J., 1967, Wall rock alteration, *in* Barnes, H.L. ed., Geochemistry of hydrothermal ore deposits: New York, Holt, Rinehart and Winston, Inc., p. 166–232.

Meyer, C., Shea, E., Goddard, C., and staff, 1968, Ore deposits at Butte, Montana, *in* Ridge, J.D. ed., Ore deposits of the United States 1933–1967 [Graton-Sales volume]: New York, American Institute of Mining, Metallurgical, and Petroleum Engineers, v. 2, p. 1363–1416.

Miller, B.J., 2004, Aqueous fluid inclusions in the Butte, Montana, Main stage vein system: Unpublished master's thesis, Eugene, Oregon, University of Oregon, 101 p.

Miller, R.N., ed., 1973, A field meeting held August 18–21, 1973, Butte, Montana, sponsored by the Society of Economic Geologists, U.S. Geological Survey, and Anaconda Company, Geological Department <http://books-geology.com/montana.htm>.

Muntean, J.L., and Einaudi, M.T., 2001, Porphyry-epithermal transition: Maracunga belt, northern Chile: Economic Geology, v. 96, p. 743–772.

Nash, T.J., 1976, Fluid inclusion petrology data from porphyry copper deposits and applications to exploration: U.S. Geological Survey Professional Paper 907-D, 16 p.

Nash, T.J., and Cunningham, C.G., Jr., 1974, Fluid inclusion studies of the porphyry copper deposit at Bagdad, AZ: U.S. Geological Survey Journal of Research, v. 2, no. 1, p. 31–34.

Ossandon, C.G., Freraut, C.R., and Gustafson, L.B., 2001, Geology of the Chuquicamata mine; a progress report: Economic Geology, v. 96, p. 249–270.

Parry, W.T., 1986, Estimation of XCO_2, Pressure and fluid inclusion volume from fluid inclusion temperature measurements in the system NaCl-CO_2-H_2O: Economic Geology, v. 81, p. 1009–1013.

Phillips, C.H., Smith, T.W., and Harrison, E.D., 1998, Alteration metal zoning and ore controls in the Bingham Canyon porphyry copper deposits, Utah: Society of Economic Geologists Guidebook Series v. 29, p. 133–145.

Pichavant, M., Ramboz, C., and Weisbrod, A., 1982, Fluid immiscibility in natural processes: Use and misuse of fluid inclusion data; I. Phase equilibria analysis—a theoretical and geometrical approach: Chemical Geology, v. 37, p. 1–27.

Preece, R.K., and Beane, R.E., 1982, Constrasting evolutions of hydrothermal alteration in quartz monzonite and quartz diorite wall rocks at the Sierrita porphyry copper deposit, AZ: Economic Geology, v. 77, p. 1621–1641.

Proffett, J.M., 1973, Structure of the Butte district, Montana, *in* Miller, R.N., ed., A field meeting held August 18–21, 1973, Butte, Montana: Sponsored by the Society of Economic Geologists, U.S. Geological Survey, and Anaconda Company, Geological Department, p. G1–12.

Ratcliff, M.W., 1973, Copper and molybdenum mineralization in the continental deposit, East Butte district, Montana: *in* Miller, R.N., ed., A Field Meeting held August 18–21, 1973, Butte, Montana: Sponsored by the Society of Economic Geologists, U.S. Geological Survey, and Anaconda Company, Geological Department, p. I1–I8.

Redmond, P.B., Einaudi, M.T., Inan, E.E., Landtwing, M.R., and Heinrich, C.A., 2004, Copper deposition by fluid cooling in intrusion-centered systems: New insights from the Bingham porphyry ore deposit, Utah: Geology, v. 32, p. 217–220.

Reed, M.H., 1999, Zoning of metals and early potassic and sericitic hydrothermal alteration in the Butte, Montana, porphyry Cu–Mo deposit [abs.]: Geological Society of America Abstracts with Programs, v. 31, no. 7, p. A381.

Reed, M., and Rusk, B., 2001, Insights into supercritical hydrothermal processes from numerical models of potassic hydrothermal alteration, and SEM-CL imaging of vein quartz at Butte, Montana, *in* Toshiyuki, H., ed., Proceedings from the Workshop on Potential Thermal Extraction from Deep-seated Rock Masses: Sendai, Japan, Tohoku University, p. 37–53.

Reed, M.H., Rusk, B., Palandri, J., and Dilles, J., 2005, The Butte hydrothermal system: One magmatic fluid yielded all vein types [abs.]: Geological Society of America Abstracts with Programs, v. 37, no. 7, p. A315.

Reynolds, J.T., and Beane, R.E., 1985, Evolution of hydrothermal fluid characteristics at the Santa Rita, New Mexico, porphyry copper deposit: Economic Geology, v. 80, p. 1328–1347.

Roberts, S.A., 1973, Pervasive early alteration in the Butte district, Montana, *in* Miller, R.N. ed., A Field Meeting held August 18–21, 1973, Butte, Montana: Sponsored by the Society of Economic Geologists, U.S. Geological Survey, and Anaconda Company, Geological Department, p. HH1–HH8.

——1975, Early hydrothermal alteration and mineralization in the Butte district, Montana: Unpublished Ph.D. dissertation, Harvard University, 157 p.

Roedder, E., 1971, Fluid inclusion studies on the porphyry-type ore deposits at Bingham, Utah, Butte, Montana, and Climax, Colorado: Economic Geology, v. 66, p. 98–120.

——1984, Fluid inclusions: Reviews in Mineralogy, v. 12, 646 p.

Rosso, K.M., and Bodnar, R.J., 1995, Microthermometric and Raman spectroscopic detection limits of CO_2 in fluid inclusions and the Raman spectroscopic characterization of CO_2. Geochimica et Cosmochimica Acta, v. 59, p. 3961–3975.

Rusk, B.G., 2003, Cathodoluminescent quartz textures and fluid inclusions in veins of the porphyry copper-molybdenum deposit in Butte, Montana: Constraints on the physical and chemical evolution of the hydrothermal system, Unpublished Ph.D. dissertation, Eugene, Oregon, University of Oregon, 285 p.

Rusk, B.G., and Reed, M.H., 2002, Scanning electron microscope-cathodoluminescence of quartz reveals complex growth histories in veins from the Butte porphyry copper deposit, Montana: Geology, v. 30, p. 727–730.

Rusk, B., Reed, M., Dilles, J.H., Klemm, L., and Heinrich, C.A., 2004, Compositions of magmatic hydrothermal fluids determined by LA-ICP-MS of fluid inclusions from the porphyry copper-molybdenum deposit at Butte, Montana: Chemical Geology, v. 210, p. 173–199.

Rusk, B.G., Landis, G., Hunt, A.G., Hofstra, A., Reed, M.H., Dilles, J.H., and Rye, R.O., 2005, Origin and evolution of hydrothermal fluids that formed the porphyry Cu-Mo deposit in Butte, Montana: A multi-faceted fluid inclusion study [abs.]: Geological Society of America Abstracts with Programs, v. 37, no. 7, p. A315.

Rusk, B., Reed, M., Dilles, J., and Kent, A., 2006, Intensity of quartz cathodoluminescence and trace element content of quartz from the porphyry copper deposit in Butte, Montana: American Mineralogist, v. 91, p. 1300–1312.

Rusk, B.G., Hofstra, A.H., Emsbo, P., Hunt, A.G., Landis, G.P., and Rye, R.O., 2007, Origin and compositions of fluids that form porphyry copper (Au-Mo) deposits [abs.]: Geological Society of America Abstracts with Programs, v. 39, no. 6, p. 608.

Sales, R.H., 1914, Ore deposits at Butte, Montana: American Institute of Mining and Metallurgical Engineers, Transactions, v. 46, p. 3–109.

Sales, R., and Meyer, C., 1948, Wall rock alteration at Butte: American Institute of Mining and Metallurgical Engineers, Transactions, v. 46, p. 4–106.

Schmidt, C., and Bodnar, R.J., 2000, Synthetic fluid inclusions: XVI. PVTX properties in the system H_2O-NaCl-CO_2 at elevated temperatures, pressures, and salinities: Geochimica et Cosmochimica Acta, v. 64, p. 3853–3869.

Seedorff, E., and Einaudi, M.T., 2004, Henderson porphyry molybdenum system, Colorado: II Decoupling of introduction and deposition of metals during geochemical evolution of hydrothermal fluids: Economic Geology, v. 99, p. 39–72.

Seedorff, E., Dilles, J.H., Proffett, J.M., Einaudi, M.T., Zurcher, L., Stavast, W.J.A., Johnson, D.A., and Barton, M.D., 2005, Porphyry deposits: Characteristics and origin of hypogene features: Economic Geology 100th Anniversary Volume, p. 251–298.

Sheppard, S.M.F., and Gustafson, L.B., 1976, Oxygen and hydrogen isotopes in the porphyry copper deposit at El Salvador, Chile: Economic Geology, v. 71, p. 1549–1559.

Sheppard, S.M.F., and Taylor, J.P., 1974, Hydrogen and oxygen isotope evidence for the origins of water in the Boulder batholith and the Butte ore deposits, Montana: Economic Geology, v. 69, p. 926–946.

Simon, A.C., Pettke, T., Candela, P.A., Piccoli, P.M., Heinrich, C., 2006, Copper partitioning in a melt-vapor-brine-magnetite-pyrrhotite assemblage: Geochimica et Cosmochimica Acta, v. 70, p. 5583–5600.

Smedes, H.W., 1973, Regional geologic setting of the Boulder batholith, Montana, *in* Miller, R.N. ed., A Field Meeting held August 18-21, 1973, Butte, Montana: Sponsored by the Society of Economic Geologists, U.S. Geological Survey, and Anaconda Company, Geological Department, sec. A.

Snee, L., Miggins, D., Geissman, J., Reed, M., Dilles, J., and Zhang, L., 1999, Thermal history of the Butte porphyry system, Montana [abs.]: Geological Society of America Abstracts with Program, v. 31, p. 380.

Sourirajan, S., and Kennedy, G.C., 1962, The system H_2O-NaCl at elevated temperatures and pressures: American Journal of Science, v. 260, p. 115–141.

Sterner, M., 1992, Homogenization of fluid inclusions to the vapor phase: The apparent homogenization phenomenon: Economic Geology, v. 87, p. 1616–1623.

Sterner, S.M., and Bodnar, R.J., 1984, Synthetic fluid inclusions in natural quartz. I. Compositional types synthesized and applications to experimental geochemistry: Geochimica et Cosmochimica Acta, v. 48, p. 2659–2668.

Takenouchi, S., and Kennedy, G.C., 1965, The solubility of carbon dioxide in NaCl solutions at high temperatures and pressures: American Journal of Science, v. 263, p. 445–454.

Taylor, H.P., 1997, Oxygen and hydrogen isotope relationships in hydrothermal mineral deposits, *in* Barnes, H.L. ed., Geochemistry of hydrothermal ore deposits, 3rd ed: New York, John Wiley and sons, p. 229–302.

Tilling, R.I., 1973, The Boulder batholith, Montana: Product of two contemporaneous, but chemically and isotopically distinct magma series: *in* Miller, R.N. ed., A Field Meeting held August 18-21, 1973, Butte, Montana: Sponsored by the Society of Economic Geologists, U.S. Geological Survey, and Anaconda Company, Geological Department, sec. C.

Tilling, R.I., Klepper, M.R., Obradovich, J.D., 1968, K-Ar ages and time span of emplacement of the Boulder batholith, Montana: American Journal of Science, v. 266, p. 671–689.

Ulrich, T., Günther, D, and Heinrich, C.A., 2001, The evolution of a porphyry Cu-Au deposit based on LA-ICP-MS analyses of fluid inclusions: Bajo de la Alumbrera, Argentina: Economic Geology, v. 96, p. 1743-1774.

Urusova, M.A., 1975 Volume properties of aqueous solutions of sodium chloride at elevated temperatures and pressures: Russian Journal of Inorganic Chemistry, v. 20, p. 1717–1721.

Wang, Y., Sasaki, M., Sasada, M., and Chen, C., 1999, Fluid inclusion studies of the Chinkuashih high-sulfidation gold-copper deposits in Taiwan; Pan-American conference on research on fluid inclusions: Chemical Geology, v. 154, p. 155–167.

Wanhainen, C., Broman, C., and Martinsson, O., 2003, The Aitik Cu-Au-Ag deposit in northern Sweden; A product of high salinity fluids: Mineralium Deposita, v. 38, p. 715–726.

Wark, D.A., and Watson, E.B., 2006, TitaniQ: A titanium-in-quartz geothermometer: Contributions to Mineralogy and Petrology, v. 152, p. 743–754.

Watanabe, Y., and Hedenquist, J.W., 2001, Mineralogic and stable isotope zonation at the surface over El Salvador porphyry copper deposit, Chile: Economic Geology, v. 96, p. 1775–1797.

Weed, W.H., 1912, Geology and ore depositions of the Butte district, Montana: U.S. Geological Survey Professional Paper 74, 262 p.

White, W.H., Bookstrom, A.A., Kamilli, R.J., Ganster, M.W., Smith, R.P., Ranta, D.E., and Steininger, R.C., 1981, Character and origin of Climax-type porphyry molybdenum deposits: Economic Geology 75th Anniversary Volume, p. 270–316.

Wiebe, R.A., 1996, Mafic-silicic layered intrusions: The role of basaltic injections on magmatic processes and the evolution of silicic magma chambers: Transactions of the Royal Society of Edinburgh: Earth Sciences, v. 87, p. 233–242.

Zhang, L., 2000, Stable isotope investigation of a hydrothermal alteration system; Butte porphyry copper deposit: Unpublished Ph.D. dissertation, Corvallis, Oregon, Oregon State University, 182 p.

Zhang, L., Dilles, J.H., Field, C.W., and Reed, M.H., 1999, Oxygen and hydrogen isotope geochemistry of pre-Main stage porphyry Cu-Mo mineralization at Butte, Montana [abs.]: Geological Society of America Abstracts with Programs, v. 31, no. 7. p. A381.

Zotov, A.V., Kudrin, A.V., Levin, K.A., Shikina, N.D., and Varyash, L.N., 1995, Experimental studies of the solubility and complexing of selected ore elements (Au, Ag, Cu, Mo, As, Sb, Hg) in aqueous solutions, *in* Shmulovich, K.I., Yardley, B.W.D., and Gonchar, G.A., eds, Fluids in the crust: Equilibrium and transport properties: London, Chapman and Hall, p. 95–138.